

Estimation of Water Infiltration into Dune Sands of Saudi Arabia by  
Using Large Scale TDR Sensors

Andreas Meier



Institute of Geography

Chair of Physical Geography / Regional Geography of Central Europe

# **Estimation of Water Infiltration into Dune Sands of Saudi Arabia by Using Large Scale TDR Sensors**

Diploma thesis submitted to achieve the degree of a  
Diplom-Geograph

supervisors:

Prof. Dr. A. Kleber, Technische Universität Dresden

Dr. T. Rödiger and Dr. C. Siebert, Helmholtz-Centre for Environmental Research UFZ

submitting by:

**Andreas Meier**

Date of birth: June, 30 1982

matriculation number: 2934947

Halle (Saale), October 20, 2011

# Contents

<b>List of Figures</b>	<b>iv</b>
<b>List of Tables</b>	<b>v</b>
<b>Listings</b>	<b>vi</b>
<b>1. Introduction - Demand and Supply of Water in Arid Regions</b>	<b>1</b>
<b>2. Objectives of the Thesis</b>	<b>2</b>
<b>3. Classification of the Study Area</b>	<b>3</b>
<b>4. Principles of Time Domain Reflectometry</b>	<b>5</b>
4.1. General Basics of TDR Technique . . . . .	5
4.2. Appliance of TDR . . . . .	7
<b>5. Methods</b>	<b>10</b>
5.1. Analysis of TRMM Data . . . . .	10
5.2. Realization of the Field Experiment . . . . .	12
5.3. Laboratory Analysis . . . . .	16
5.3.1. Analyses of Field- and Laboratory Sand Dielectrics . . . . .	18
5.3.2. Experimental Pretests . . . . .	19
5.3.3. Construction of own TDR Sensors . . . . .	22
5.3.4. Calibration Setup for the Taupe and Tube Sensor . . . . .	22
<b>6. Results and Discussion</b>	<b>25</b>
6.1. Climate and Weather Analyzes . . . . .	25
6.1.1. Results of TRMM Data Analyzes . . . . .	25
6.1.2. Weather and Soil Temperature of the Test Field . . . . .	26
6.2. Calibration Results . . . . .	27
6.2.1. Soil Moisture Content with TDR Short Rod Sensor Z 5 . . . . .	27
6.2.2. Integral Soil Moisture Content with Taupe and Tube Sensor . . . . .	29

6.2.3. Spatial Distribution of Soil Water Content . . . . .	32
6.3. Integral Soil Moisture of TDR Field Measurements . . . . .	38
6.4. Analysis of Measured Reflection Coefficients in a Spatial Context . . .	40
6.5. Modeling Soil Moisture Contents . . . . .	43
<b>7. Conclusion of the Thesis</b>	<b>48</b>
<b>8. Final Consideration and Future Prospects</b>	<b>50</b>
<b>Bibliography</b>	<b>50</b>
<b>A. Appendix</b>	<b>54</b>

## List of Figures

3.1. General pattern of isohyets over Saudi Arabia. . . . .	4
4.1. Arrangement of TDR hardware and two three rod sensors. . . . .	8
4.2. Traveling time of a waveform derived between a and b. . . . .	9
4.3. Expanding signals in wet and dry sand in travel time and the amplitude of the reflection coefficient. . . . .	9
5.1. Situation of the TRMM pixel. . . . .	11
5.2. Preparation of the liners in the field. . . . .	13
5.3. Construction of the Tube sensor on the test site. . . . .	14
5.4. Installation and sensor setup of TAUPE sensor. . . . .	15
5.5. Arrangement of the TDR sensors on the test field. . . . .	17
5.6. Overview to the test site on Al-Adel farm. . . . .	18
5.7. $K_a$ measuring cylinder construction with coaxial structure. . . . .	19
5.8. Irregular distribution of moisture three days after moisturization. . . .	20
5.9. Finished setup of the second experiment with the additional five short rod TDR sensors during the irrigation process from the bottom, just before saturation. . . . .	21
5.11. Travel time of sensor Z 5 between start and stop time, adjusted about the offset. . . . .	23
5.12. Calibration setup for the three sensors types. . . . .	23
5.13. Sandbox for TDR measurements and measuring technology in the right bottom corner; measure points P1–P5 with sensor Z 5. . . . .	24
6.3. Air temperature and precipitation from test field climate station; Soil temperature T1–T6. . . . .	28
6.4. Measurements of sand moisture content and adjusted calibration functions. 29	
6.5. Average results derived with 3rd degree polynomial function for P1–P5 and their standard deviation. . . . .	30
6.6. $K_a$ analysis of Taupe- and Tube sensor. . . . .	30

6.7. Calibration for Taupe- and Tube sensor. . . . .	31
6.8. Calculation of volumetric water content with the calibration functions 6.2 and 6.3. . . . .	32
6.9. Taupe: 20 TDR signals from sandbox experiment II plus the signal in air: The brighter the color the longer the signal, the moister the sand. In black: TDR signal in air. . . . .	32
6.10. Tube: 20 TDR signals from sandbox experiment II plus the signal in air: The brighter the color the longer the signal, the moister the sand. In black: TDR signal in air. . . . .	33
6.11. Taupe: 20 detrended plateau parts of the original TDR signals, arrange- ment of signals analog to fig. 6.9. . . . .	34
6.12. Tube: 20 detrended plateau parts of the original TDR signals, arrange- ment of signals analog to fig. 6.9. . . . .	34
6.13. System of shortening the different long TDR-signals. . . . .	35
6.14. Calibration functions from Taupe- and Tube sensor for the reflection coefficient. . . . .	35
6.15. Taupe: Spatial distribution of sand moisture content of 20 moisturization cycles. . . . .	36
6.16. Tube: Spatial distribution of sand moisture content of 20 moisturization cycles. . . . .	36
6.17. Comparison of exemplary moisturization cycles 2, 11 and 17. . . . .	37
6.18. Ten representative TDR signals of sensor V3 between March and July. . . . .	38
6.19. Integral VWC from March till July for the vertical Taupe sensors V1 – V6. The length of the sensors is given in tab. 2.2. The ground plan of the test field positions the signals. . . . .	39
6.20. Assumed distribution of soil moisture content along the sensor. . . . .	40
6.21. Ground plan of the test field: Increase of soil moisture content from March – July; ++ high differences, -- least differences. . . . .	40
6.22. TDR-signals from sensor V3 at marked dates, before and after the most abundant precipitation events. . . . .	41
6.23. Average of reflection coefficient in the plateau period of a TDR signal. . . . .	42
6.24. Daily fluctuations of the averaged reflection coefficient from March, 29th – March, 31st. . . . .	42
6.25. Average of reflection coefficients for one meter sections of the TDR signal plateau. . . . .	43

6.26. Signals from several measurements: Originals lined, Detrended dashed.	44
6.27. Spatial resolved sand moisture content from the beginning of March till the beginning of July; Air temperature and precipitation for the same period. . . . .	45

## List of Tables

1.1.	TRMM coordinates for the observed area. . . . .	10
2.1.	Soil temperature sensors on the test site. . . . .	15
2.2.	TDR sensors of the field experiment. . . . .	16
3.1.	$K_a$ of desert sand. . . . .	19
2.1.	Constant travel times for Taupe- and Tube sensor, the travel time in air is offset corrected. . . . .	29
A.1.	Added tap water in the single moisturization cycles (chapter 5.3.4). . .	57
A.2.	VWC of Z 5: Thermogravimetric results, calculation with Topp's equation and a 3rd order polynomial as well as theoretical VWC calculated from controlled water add-on, according graph in fig. 6.4, pg. 29. . . .	58
A.3.	Calculated volumetric water content from chapter 6.2.1, measured with sensor Z 5, the values are displayed in fig. 6.4 and 6.5. . . . .	59
A.4.	Travel time and $K_a$ of Taupe sensor measures in sandbox experiment II, travel time in air and offset in tab. 2.1, pg. 29, VWC ( $\Theta_{vol}\%$ ) calculated with equation 6.2. . . . .	60
A.5.	Travel time and $K_a$ of Tube sensor measures in sandbox experiment II, travel time in air and offset in tab. 2.1 pg. 29, VWC ( $\Theta_{vol}\%$ ) calculated with equation 6.2. . . . .	61
A.6.	Physical length of the Tube sensors compared to its travel times in air ( $t_l$ ). . . . .	61

## Listings

A1.1.Source code for 11 TAUPE-TDR-Sensors and 7 temperature sensors CS T107 in crbasic for Campbell Scientific Datalogger CR1000, edited by Franz Königer at August, 10th 2009, modified by Andreas Meier, at October, 18th 2010. . . . .	54
--	----

## Nomenclature

$\bar{\rho}$	.....	average of reflection coefficients
$\rho$	.....	reflection coefficient
$\Theta_{vol}\%$ , VWC	...	volumetric water content percent
EC	.....	electro conductivity
eq.	.....	Equation
fig.	.....	Figure
$K_a$	.....	apparent dielectric constant
pg.	.....	Page
tab.	.....	Table
TDR	.....	Time Domain Reflectometry

# 1. Introduction - Demand and Supply of Water in Arid Regions

*“Access to safe water is a fundamental human need and therefore a basic human right. [...] In this new century, water, its sanitation, and its equitable distribution, pose great social challenges for our world. We need to safeguard the global supply of healthy water and to ensure that everyone has access to it.”*

*Kofi Annan, UN general meeting New York, March 22 2002*

The United Nations proclaimed the 15 millennium goals in 2002. The seventh goal of them claims to “ensure environmental sustainability” (UN, 2010). Special emphasize was given to the unsustainable exploitation of water resources. During the last 100 years the consumption of freshwater increased sixfold while the world’s population “just” doubled. Today approximately one third of humanity lives in “water stressed countries”. If development turns on as today, it will be two fifth by 2025 (UN, 2002).

Saudi Arabia, as a part of the Arabian peninsula is one of these water stressed countries. An increasing population and a higher living standard as well as modern technical opportunities lead to a higher water consumption. The overexploitation of “fossil” groundwater resources affects the aquifers productivity – in quantity as well as in quality (Al-Rashed and Sherif, 2000). For that reason a sustainable water management must be developed, which is based on a protection of available water resources.

The approach of the IWAS project (*I*nternational *W*ater Research *A*lliance *S*axony) is to estimate groundwater recharge for the middle east region. It is important to understand the behavior of water in the vadose zone because precipitation is only episodic. This study is based on Time Domain Reflectometry (TDR) measurements. The method allows a high resolution monitoring of the moving process of infiltrated water in a field experiment in Saudi Arabia.

## 2. Objectives of the Thesis

Only few studies deal with the process of water infiltration through the vadose zone in arid regions (Dincer et al., 1974, S. 79). A survey to recent studies is even given in Subyani (2005).

The aim of the presented study is to understand the groundwater recharge for representative local conditions in Saudi Arabia. Therefore a test site on a sandy substrate was searched, because sandy dunes represent 60-80 percent of the main land coverage of the country. That is an area larger than France.

The process of recharge is dependent of atmospheric processes like precipitation and evaporation as well the infiltration. To estimate the recharge it is necessary to know the ratio between these parameters. The following questions could be derived:

1. *Which amount of a precipitation event leads to groundwater recharge and how long does it take?*
2. *Is a point of no return available and in which depth is it located?*
3. *How much time is required to evaporate soil moisture above this point?*

To solve these questions a test field was installed, consisting of several measuring systems (chapter 5.2).

TDR probes were installed to measure the soil moisture content. Two different sensor types were used. The individual setup of the sensors required a specific calibration for each. The challenge was to transfer the reflected signal to a realistic water content. The technical question was posed:

4. *What is the calibration function for each sensor?*
5. *How can a spatial resolution be achieved along the sensor?*

### 3. Classification of the Study Area

Saudi Arabia is part of the middle east and with its size of 2.149.690 km<sup>2</sup> it covers 80% of the Arabian peninsula (Central Intelligence Agency, 2011). From north it clockwise borders on Jordan, Iraq, Kuwait, the United Arabian Emirates, Oman and Yemen. Its natural borders are the Arabian gulf in the East and the Red Sea in the West.

The natural environment of Saudi Arabia can be divided into six regions: mountainous regions aside the Red Sea, highly elevated plains, a belt of downhill escarpments, the interior platform, coastal areas and sand dune areas. The last cover almost one-half of the country's surface. Two main desert areas are An' Nafud in the north of the central part and the world's largest sand desert Rub' al-Khali in the south (Shahin, 2007, pg. 66f.).

In Saudi Arabia there virtually exist no permanent rivers. Arable land can only be found in wadis, basins and oases (Britannica Online Encyclopedia, 2011).

Climatically the country can be divided in two parts. The largest part of the peninsula is dominated by warm-temperate, Mediterranean affected semitropics with precipitation only in winter. Embedded depressions in these air masses bring much of the rain (Vincent, 2008; Ministry of Agriculture and Water, 1988).

The southern part belongs to the tropical summer rain region of the marginal tropics. It gets precipitation from offshoots of the Asian monsoon. Due to the situation in the dry belt of the trade winds Saudi Arabia is arid (Barth and Schliephake, 1998, pg. 45f).

The scarcity of precipitation and the high temperatures are responsible for the characteristic deserts and semideserts. Fig. 3.1 shows that most of the country receives less than 100 mm per year (Riyadh 100.6 mm). Indeed it is possible that desert regions get no rain for several years, followed by years with much more than the mean precipitation (Barth and Schliephake, 1998, pg. 50).

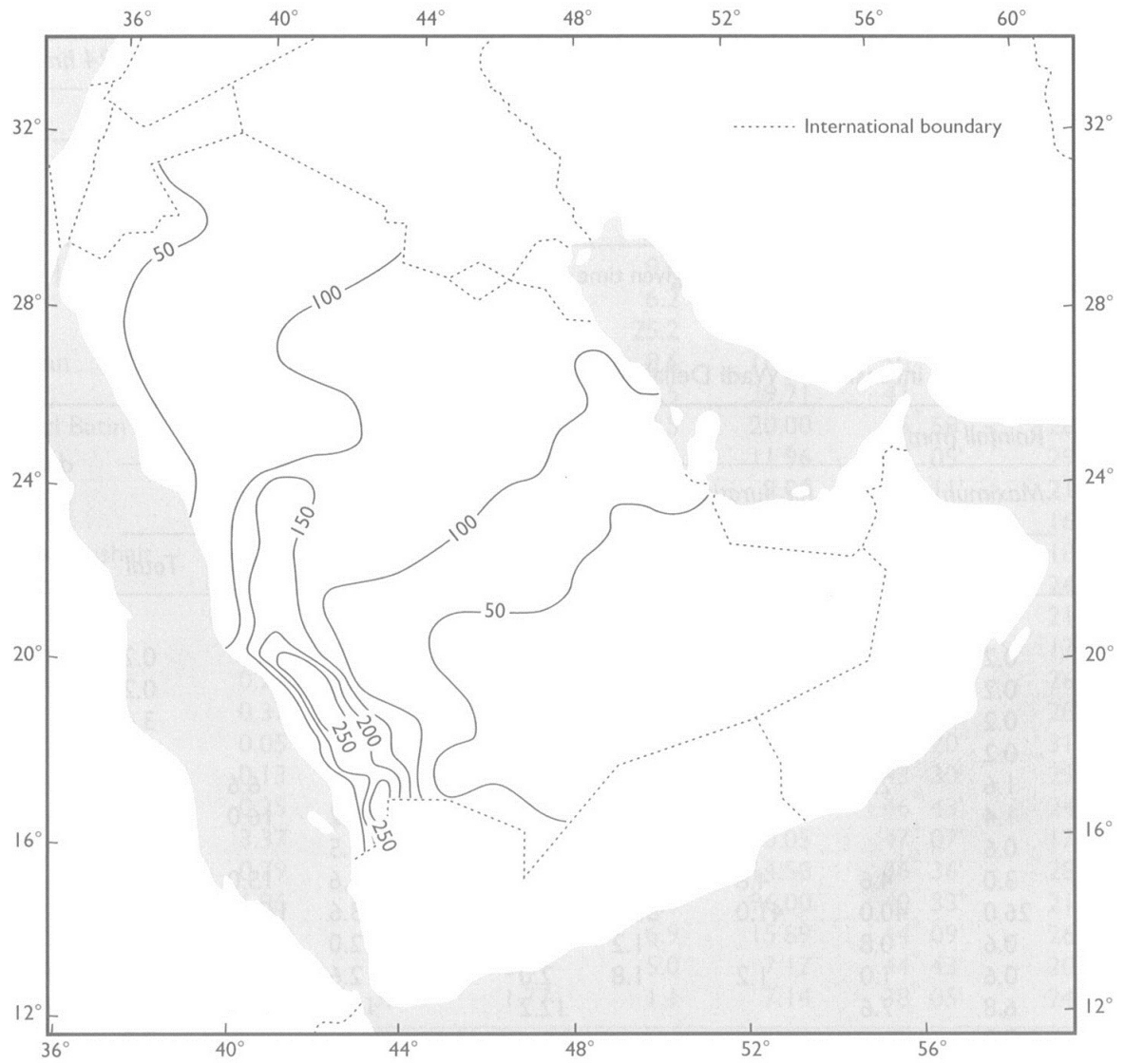


**Fig. 3.1.:** General pattern of isohyets over Saudi Arabia [mm], fig. from Vincent (2008, pg. 77).

## 4. Principles of Time Domain Reflectometry

The standard measuring of soil moisture content is the thermogravimetric method. It consists of measuring of a soil sample before and after drying with 105°C until mass stability. This method has been established as very accurate but it is even time intensive, soil destructive and can just be used in the laboratory. Therefore it is not useful for monitoring under field conditions. However for calibration purposes thermogravimetric soil moisture detection is the standard method (Roth et al., 1990; Kaatz and Hübner, 2010).

Time Domain Reflectometry (TDR) is an indirect measuring method, that allows to transfer a relation of propagation velocities of an electronic impulse to water content. The idea is based on Davis and Chudobiak (1975).

The advantage of TDR is the possibility to measure continuously over a period of time without modifying the soil itself. It is one of the favored methods for monitoring issues especially because it can be installed autarkically.

### 4.1. General Basics of TDR Technique

The dielectric behavior of a material is characterized by its permittivity to an electrical field. In a vacuum the permittivity ( $\epsilon_0$ ) is 1 and it is called the dielectric field constant. The relative permittivity ( $\epsilon_r$ ) is the relation of a permittivity in a material ( $\epsilon$ ) to the field constant  $\epsilon_0$  (equation 4.1)(Dirksen, 1999).

$$\epsilon_r = \frac{\epsilon}{\epsilon_0} \quad (4.1)$$

The permittivity primarily depends on the polarization of an electrical field. The dipole character of water molecules leads at 18°C to the value  $\epsilon_{\text{water}} \approx 80$ . Soil components have a markedly lower value  $\epsilon_{\text{soil}} \approx 5$ . Referring to that great difference the volumetric water content ( $\Theta_{\text{vol}}\%$ ) can be measured indirectly.

The propagation velocity of a TDR signal depends on the dielectric permittivity of the traveled medium. That means the propagation velocity changes while the bulk dielectric properties are changing as well (Topp et al., 1980, pg. 575).

The propagation velocity ( $V_P$ ) results from the time ( $t$ ) that an voltage pulse need to travel a probe forth and back (equation 4.2).

$$V_P = \frac{2l_P}{t} \quad (4.2)$$

The  $V_P$  equates as well the relation of an electromagnetic waveform in free space ( $c$ ) and the dielectric properties of the traveled medium ( $\epsilon$ ) (equation 4.3)(Topp et al., 1980).

$$V_P = \frac{c}{\sqrt{\epsilon}} \quad (4.3)$$

Conversely expressed  $\epsilon$  is a function of  $c$  and  $V_P$  (equation 4.4).

$$\epsilon = \left( \frac{c}{V_P} \right)^2 \quad (4.4)$$

The complex variable  $\epsilon$  consists of a real part ( $\epsilon'$ ) that measures the polarizability of a material and an imaginary part ( $\epsilon''$ ) being related to dielectric losses (equation 4.5).

$$\epsilon = \epsilon' - \epsilon'' \quad (4.5)$$

For that reason  $\epsilon'$  is called the *apparent* dielectric constant ( $K_a$ ). The loss is not respected because the amount is insignificantly small.  $K_a$  is the measured value (equation 4.6).

$$K_a = \epsilon' \quad (4.6)$$

The combined equations 4.4 and 4.2 are expressed in equation 4.7 (O'Connor and Dowding, 1999, S. 34f).

$$K_a \approx \left( \frac{ct}{2l_P} \right)^2 \quad (4.7)$$

A soil is a mixture of grains, water and air. As mentioned above the dielectric permittivities vary to great extent. Respectively  $\epsilon_{soil} = 4-10$  (depending on the composition of the minerals),  $\epsilon_{water} \approx 81$  and  $\epsilon_{air} \approx 1$ . These values are valid at a frequency of 50 Hz and a temperature of 18°C. It can be noticed that the amount of water has a strong influence on the dielectric permittivity of the soil The great variation is distributed to the properties of the architecture of the H<sub>2</sub>O molecule (Kaatze and Hübner, 2010).

Topp et al. (1980) empirically deduced equation 4.8 to find the volumetric water content  $\theta_{vol}\%$ . It is valid for most soil types.

$$\Theta_{vol}\% = -5.3 \cdot 10^{-2} + 2.92 \cdot 10^{-2} K_a - 5.5 \cdot 10^{-4} K_a^2 + 4.3 \cdot 10^{-6} K_a^3 \quad (4.8)$$

This equation is just valid for uncoated sensors. The field used sensors consist of coated rods, that means an individual calibration was necessary (chapter 5).

In addition to the determination of the soil moisture content as an integral average along the whole sensor, the signal gives information about the spatial distribution of the water. The reflection coefficient ( $\rho$ ) can be directly correlated to volumetric water content as long as there are no changes in electrical conductivity (Evetts et al., 2005).

The relation between time domain and frequency domain is in simple terms inverse. Short times of the time domain correspond to high frequencies and the other way around (Stacheder, 1996, pg.35).

## 4.2. Appliance of TDR

TDR sensors can be constructed in different arrangements. Two or three rod configurations are usually used (Dirksen, 1999, pg.26). The design can vary, for example in probe length, rod diameter, rod spacing or rod material (O'Connor and Dowding, 1999, pg.51). To measure a travel time a high voltage pulse with a fast rise time is generated by a TDR Unit. After propagating through a COAX-cable the impulse forms an electromagnetic field in the sensor, while the soil acts as its dielectric. Every time when the pulse meets impedance changes a part of the signal reflects back to the TDR unit. Significant changes occur to the start and to the end of a sensor. The reflected signal gets received by the TDR unit and is post-processed by an analyzing software. As an intermediate step, the signal can be stored in a data logger. Fig. 4.1 shows a the combination of several TDR hardware components and two three rod sensors. The interconnected Multiplexer allows an operating system with several sensors.

In fig. 4.2 a section of a real measured TDR signal is shown. The travel time ( $t$ ) can be determined from the distance between a and b. It represents the time of the signal traveling forth and back. The beginning and the end of the signal are derived by intersections of tangents. The length of the rods and the measured time from the signal are used for the calculation of  $K_a$  (equation 4.2 and 4.7).

The travel time also includes the sensor head, which means the part where the coax-cable is physically connected to the sensor rods. The sensor head occurs *after*

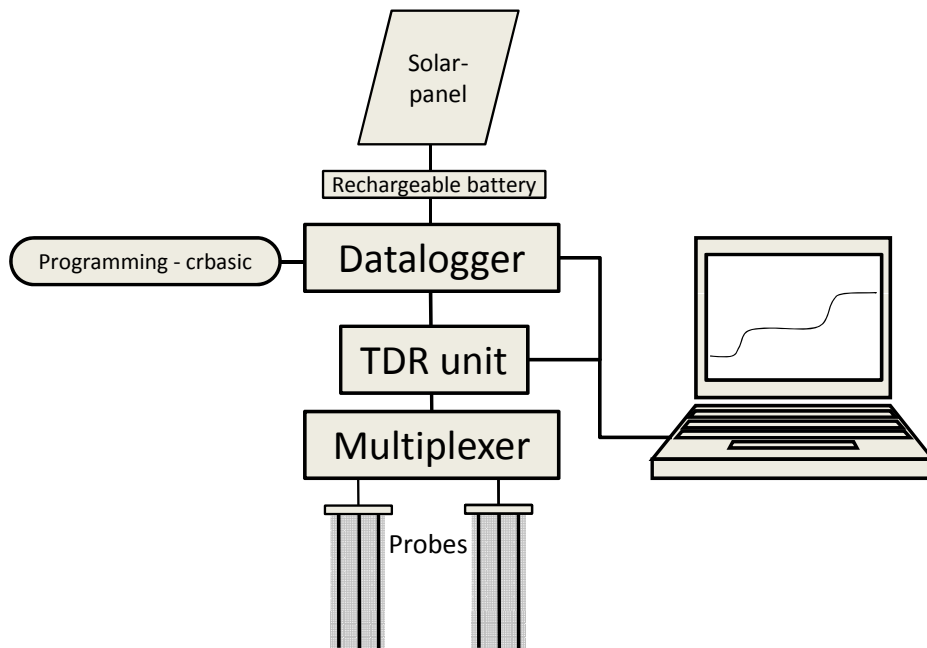


**Fig. 4.1.:** Arrangement of TDR hardware and two three rod sensors.

point “a”. It is a time constant that creates a systematic error in the calculation of the soil moisture content. With an increasing probe length it can be neglected more and more. For short sensors this value is very important, therefore this *offset* has to be subtracted from  $t$ .

Even the main characteristic parts of a TDR signal can be observed. The flat part at the beginning is proportional to the coaxial cable length and is not of interest. The first part of the significant slope represents an impedance change because of the port between coax-cable and sensor. A part of this slope is referred to as the offset, described above. The slightly waved plateau between the first and second distinctive slope represent the first reflection of the signal. The second significant slope is the end of the sensor. A total reflection occurs there. From the time distance between them  $K_a$  is calculated (Bänninger et al., 2008). After the second slope multiple reflections appear which are complex and hard to analyze (Dirksen, 1999). The software Taupe (pk tools, 2006) makes it possible to automate the positioning of the tangents and the calculation of soil moisture content.

Fig. 4.3 displays a much longer section of TDR signals. It shows two measurements of the same sensor in different moist sand. It is obvious that the signal in the wet sand is much longer as in dry sand. It is noticeable that the amplitude of the reflection coefficient decreased as well.

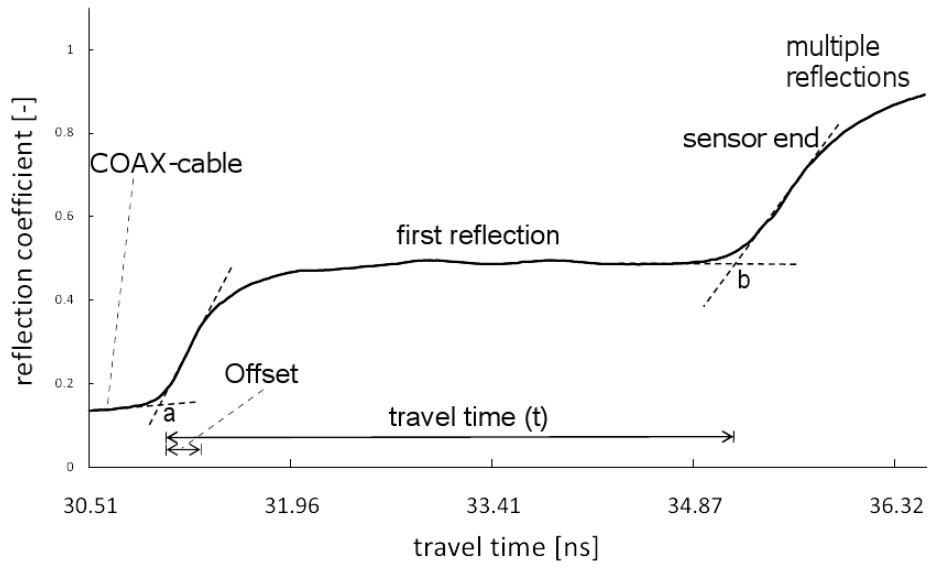


**Fig. 4.2.:** Traveling time of a waveform derived between a and b.

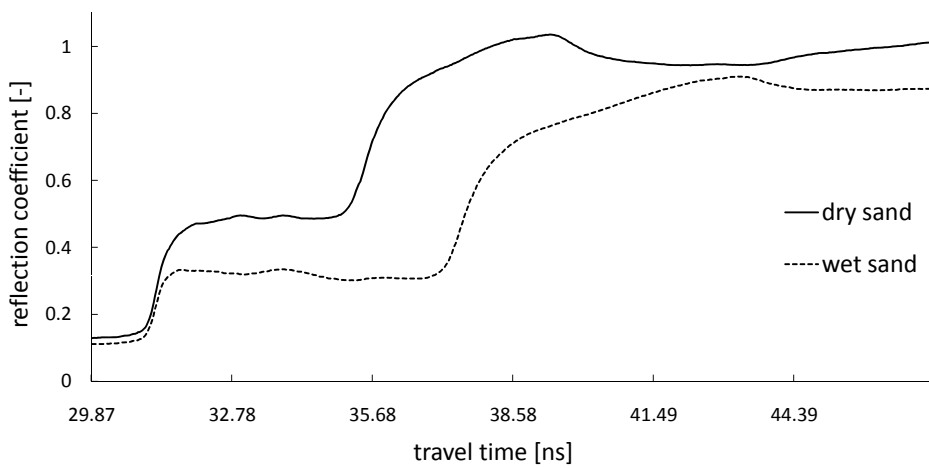


**Fig. 4.3.:** Expanding signals in wet and dry sand in travel time and the amplitude of the reflection coefficient.

## 5. Methods

### 5.1. Analysis of TRMM Data

In preparation to the field trip the question of climatic reliability of the test field was posed. To get information about the local climate TRMM<sup>1</sup>-data was analyzed to bring the local weather settings to a smaller scale context. It should be sure that the test field gets precipitation that corresponds to an average of this region.

TRMM-data is generated by a remote sensing satellite which is equipped with a precipitation radar. The radar emitted signal is reflected by water droplets and it varies with the quantity of precipitation (Römer, 2007).

The analyzed data contains of nine Pixel which are oriented as a squared grid around the test site (fig. 5.1, tab. 1.1). Each pixel has an edge length of 50 km. Cumulatively that corresponds to 22.500 km<sup>2</sup> or approximately the size of Saxony-Anhalt. The period of observing expands over ten years from 1998 till 2008. Earlier data were not available because TRMM was initially started in 1997.

**Tab. 1.1.:** TRMM coordinates for the observed area.

PixelID	Latitude	Longitude
1	24.625	45.625
2	24.625	45.875
3	24.625	46.125
4	24.375	45.625
5	24.375	45.875
6	24.375	46.125
7	24.125	45.625
8	24.125	45.875
9	24.125	46.125

---

<sup>1</sup>TRMM: Tropical Rainfall Measuring Mission

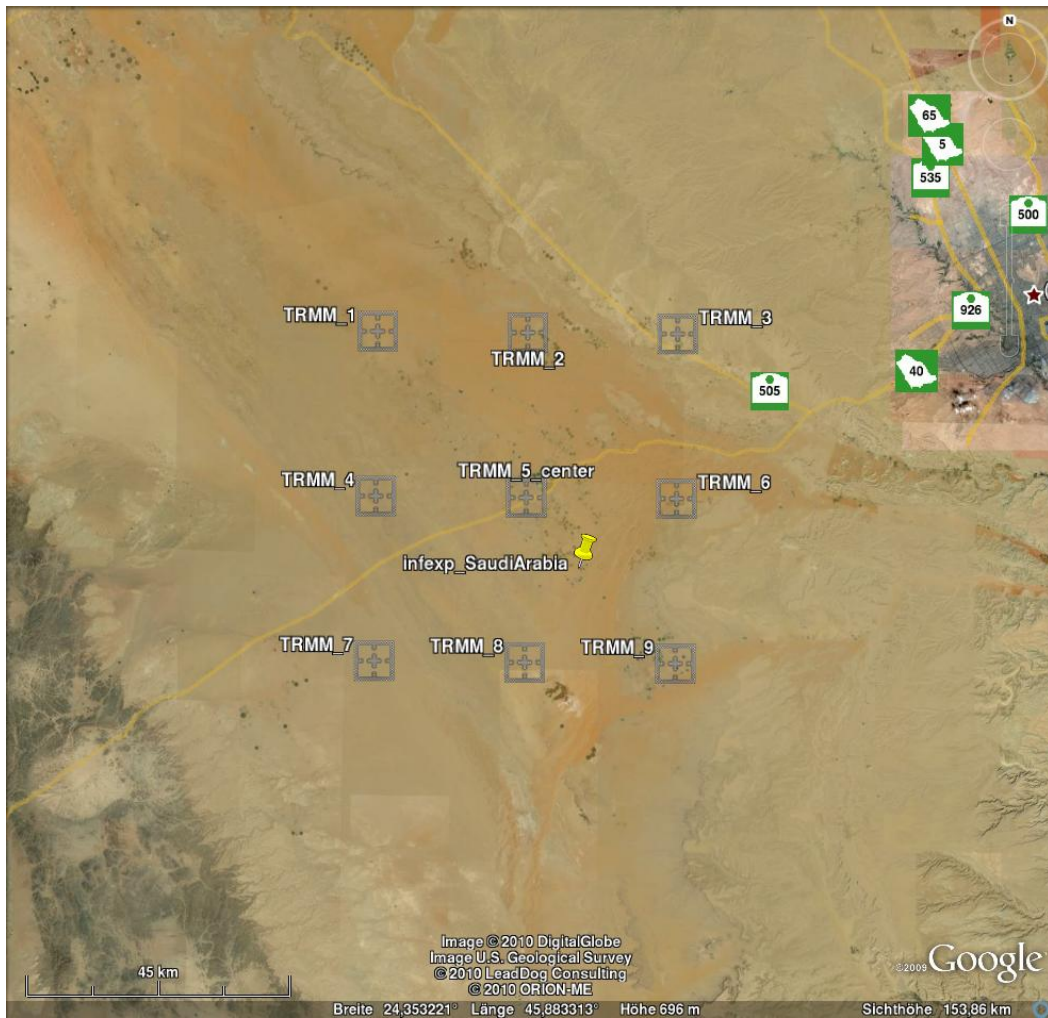


**Fig. 5.1.:** Situation of the TRMM pixel: the cross line marker flags the center of the the pixel; top right corner (NE): Riyadh; area crossing route: Mecca road; photo with google earth.

## 5.2. Realization of the Field Experiment

The main objective of the study is to understand the groundwater recharge process under local conditions in a representative area in Saudi Arabia. The best requirements for these purposes offered a sand field on a the Al-Adel farm 130 km southwestward from Riyadh.

The design of the constructed test field consists of two diagonal main TDR sensors between the long sides of the field and six vertical TDR-sensors. The last give information about water infiltration and lateral discharge during artificial irrigation experiments.

The *Tube* sensor is a development of Dr. A. Kallioras and Dr. M. Piepenbrink, both from TU Darmstadt (patent under submission, described in Schüth et al. (2010)). It consists of a solid HDPE<sup>2</sup>- tubes with three inserted, parallel running, copper varnished wires.

The *Taupe* sensor is a flat ribbon cable with three parallel rods coated by Polyethylene, precisely described in Stacheder et al. (2009, pg. 3f). In the field and consequently in the laboratory this sensor was connected to a fire hose and a HDPE-tube that was used for the other sensor.

The drilling and sampling in the field campaign was executed with a Geoprobe® 7730DT. The soil samples were gathered in hollow plastic liners. The one meter long sample tubes were cut to  $\approx 30$  cm sections and closed with rubber plugs and isolation tape to avoid evaporation (fig. 5.2a).

Several individual checks of the soil samples showed, that moisture content steplike increased strongly in a depth of about half a meter. From there the soil moisture increased just little to greater depths. Fig. 5.2b shows sand that was taken from about one meter depth. It is plastic and cohesive which is a marker of moisture content.

After the field campaign the samples should be analyzed to examine the current soil moisture content and salts for the day of installing the sensors.

The idea was to separate specific characteristics of the sensor from soil moisture content. With respect to customs problems and shipping of the liners the possibility omitted to analyze the samples. A project partner from TU Darmstadt currently deals with the interpretation of their moisture contents.

When soil sampling was terminated the sensors were installed in the still open bore holes. The following procedure was done for each sensor again.

---

<sup>2</sup>HDPE: high density polyethylene

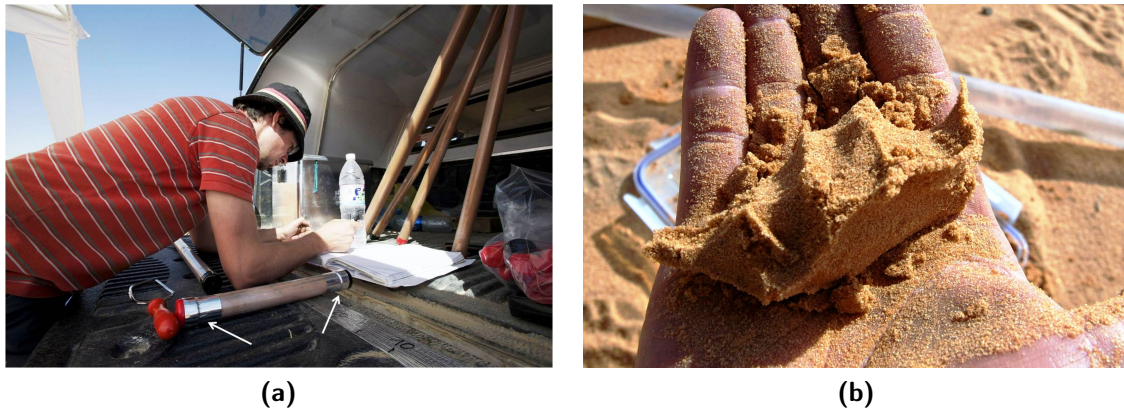


**Fig. 5.2.:** Preparation of the liners in the field with plugs and isolation tape (a) and a cohesive, moist sand, taken from one meter depth (b).

The one meter tubes consist of three parallel milled channels. After the one meter long tube pieces had been pushed into the ground one by another, three copper wires were glued to these channels continuously. Thus it was possible to arrange the wires in a constant distance next to each other. Cable straps served as temporary fixations. After the installation the three wires were connected to a  $50\ \Omega$  coaxial cable. The sensor head was sealed by a thick plug of hot glue. This procedure was repeated for all six sensors on the test site.

For measurements in the central part of the test field two ten meter long Taupe TDR-sensors were installed.

This was realized in a bore hole with a  $45^\circ$  angle by rotary dry drilling. To keep the bore hole open a steel casing was pushed through the hole while drilling (fig. 5.4a). The intention for the diagonal installation was to minimize fingering effects from water along the sensor. Fingering is discussed in chapter 5.3.2. Another advantage are the undisturbed sediments above the sensor. A disadvantage is the higher technical complexity and a longer time duration of the construction.

Prior to the experiment it was planned to fix the two ten meter Taupe sensors one after another on an inflatable, flexible sleeve like Dahan (2003) suggested. After inserting the loose sleeve-sensor combination, the sleeve should be filled with sand. The sleeve should expand to place the sensor as close as possible to the sediment.

However, after a not planned drilling width correction, the design of the sensor-sleeve combination could not be realized and had to be adjusted. The Taupe cable was fixed to a 21 m long, rigid HDPE-tube with cable binders. Between the tube and the sensor a part of the sleeve remained (fig. 5.4b).

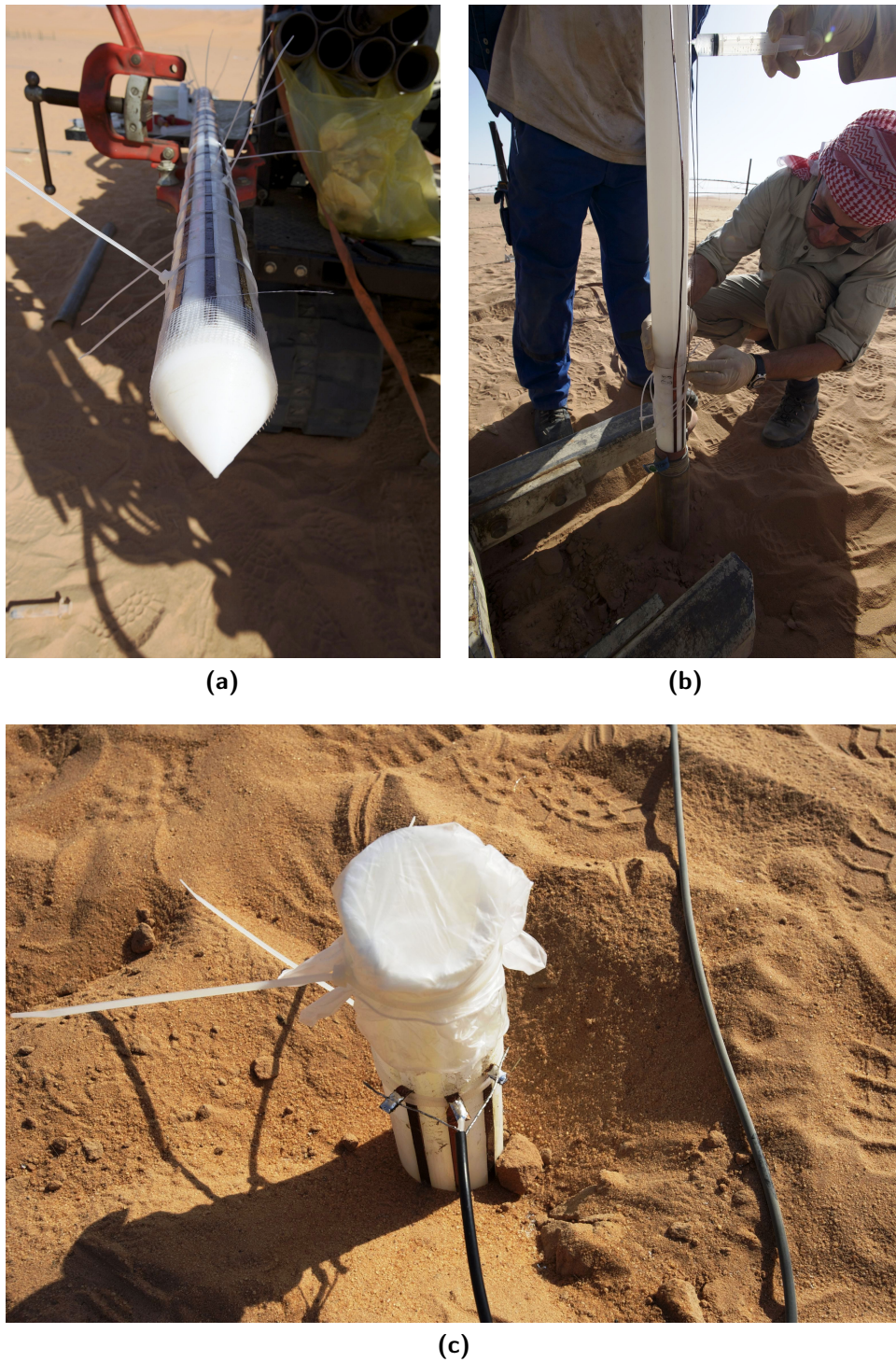


**Fig. 5.3.:** Construction of the Tube sensor on the test site: Lower end of the Tube sensor as the first step of construction (a); the installation with permanent fixation with a glue syringe and cable straps while pushing the sensor to the ground (b) and the nearly finished probe with coaxial cable but without sensor head sealing (c).

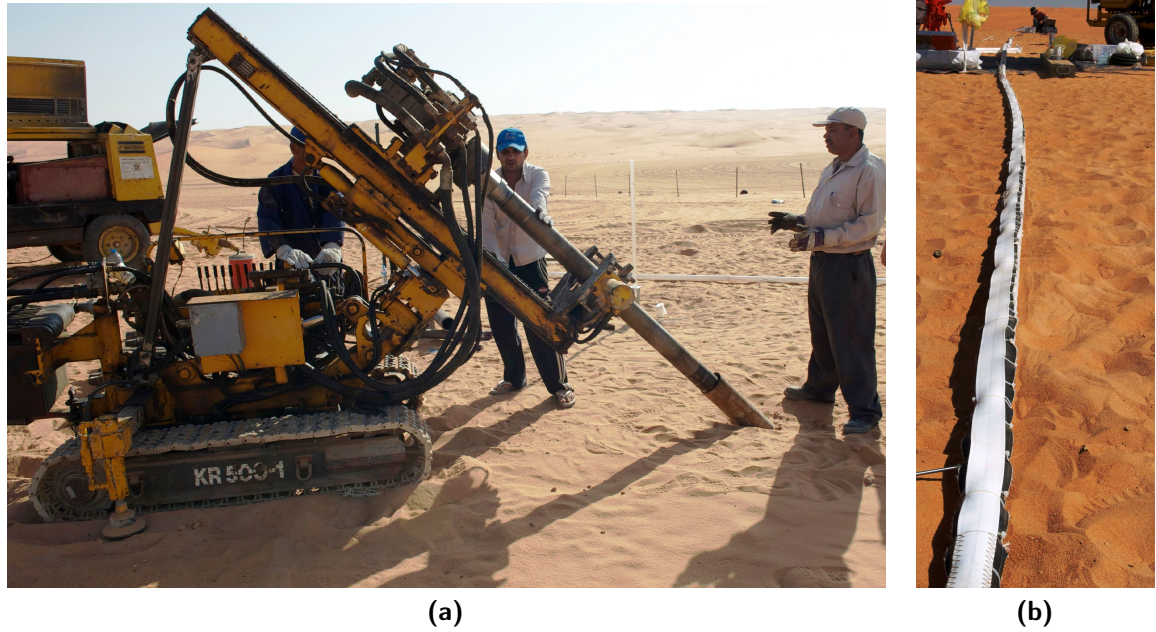


**Fig. 5.4.:** Dry drilling in a  $45^\circ$  angle (a) and final probe setup of Taupe sensor (b), the left bottom corner shows one of six temperature sensors.

Similarly six Campbell® Scientific 107 L soil temperature sensors were fixed to the opposite side of the tube to be sure not to affect the dielectric of the sensor. An overview to the final depth under earth's surface is given in table 2.1.

**Tab. 2.1.:** Soil temperature sensors on the test site.

No.	name	depth [m]
1	T1	0.5
2	T2	2.2
3	T3	3.3
4	T4	6.8
5	T5	9.8
6	T6	15.4

The rigid tube construction was pushed by hand into the open bore hole. Table 2.2 shows the arrangement and spatial situation of all TDR sensors.

All sensors are connected to coaxial cables which are again connected to a TDR reflectometer TDR 100. Two multiplexers (SDMX50), and a data logger CR 1000 complete the TDR system<sup>3</sup>. The source code for the monitoring program can be found

<sup>3</sup>All hardware by Campbell® Scientific

**Tab. 2.2.:** TDR sensors of the field experiment.

no.	name	direction of installation	length	vertical length from soil surface
1	S T1	diagonal	10.00 m	1.13 m – 8.20 m
2	S T4	diagonal	10.00 m	8.20 m – 15.27 m
3	S B	diagonal	1.00 m	0.0 m – 0.70 m
4	V1	vertical	7.74 m	0.0 m – 7.74 m
5	V2	vertical	5.14 m	0.0 m – 5.14 m
6	V3	vertical	6.30 m	0.0 m – 6.30 m
7	V4	vertical	6.40 m	0.0 m – 6.40 m
8	V5	vertical	5.65 m	0.0 m – 5.65 m
9	V6	vertical	5.15 m	0.0 m – 5.15 m

in the listings A1.1. The sketch in fig. 5.5 shows the current arrangement of all TDR - sensors on the test field.

The data logger was programmed to measure once an hour. After one month the interval was extended to four hours. After initial problems with the logger the system of nine TDR sensors and six temperature sensors has been working steadily from February 28th, 2011 till this day.

A Thies Clima weather station was constructed to measure atmospheric conditions. Sensors were installed to detect global radiation, albedo, wind direction, wind velocity, atmospheric pressure and precipitation.

An irrigation field above the arrangement completed the test field.

The field work was realized during four weeks of November 2010 and again two weeks of February 2011. An overview of the test field is given in fig. 5.6.

### 5.3. Laboratory Analysis

The greatest part of the diploma thesis dealt with the calibration of the sensors. The calibration is necessary to get valid information about the volumetric water content of the observed sensors.

For that purpose various setups were tested. The Taupe- tube construction as well as the tube sensor from TU- Darmstadt were used as the basic components. The only changed parameter was the length. The Taupe sensor was 80 cm, the Tube-sensor 100 cm long.

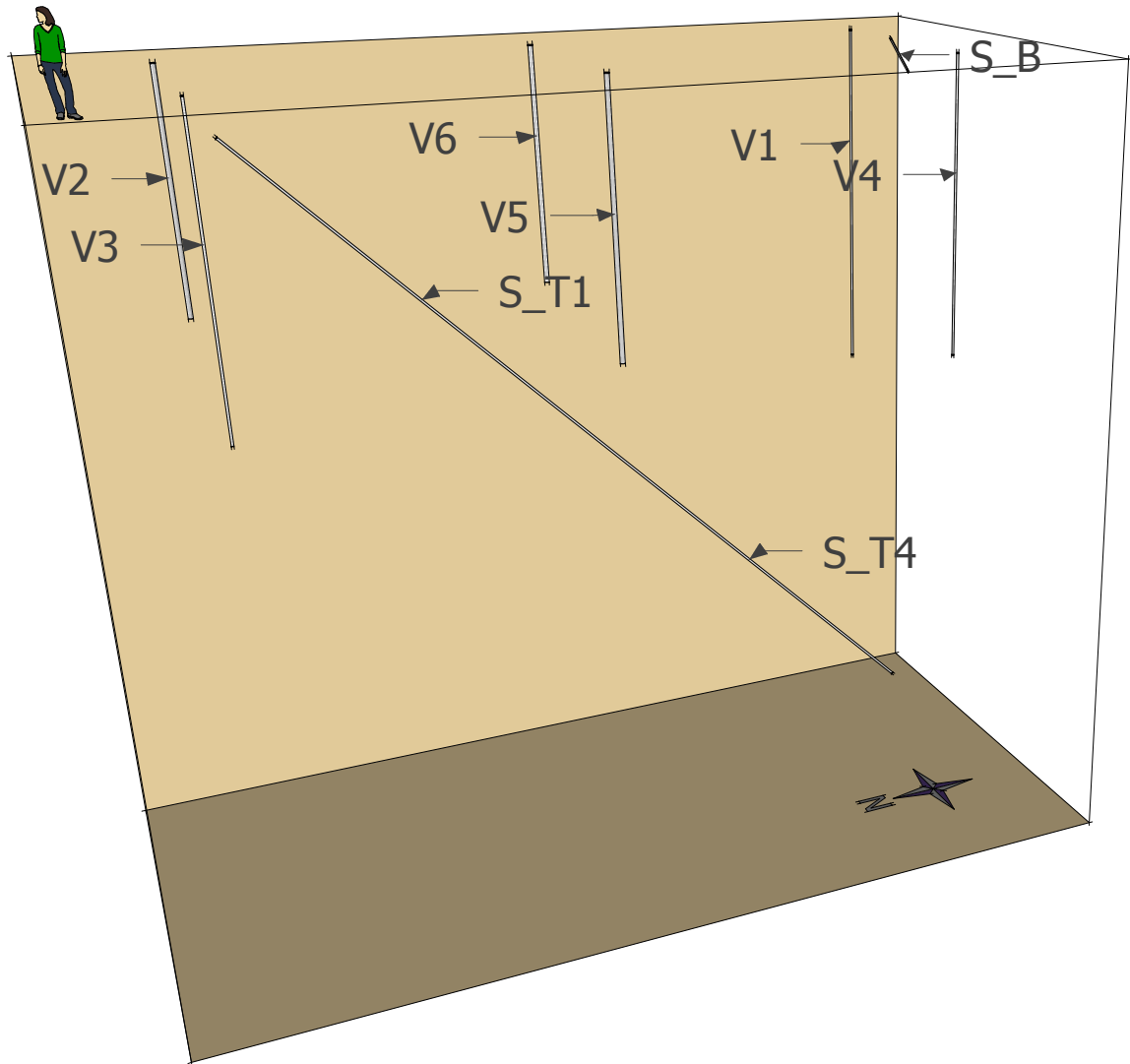


**Fig. 5.5.:** Arrangement of the TDR sensors on the test field.

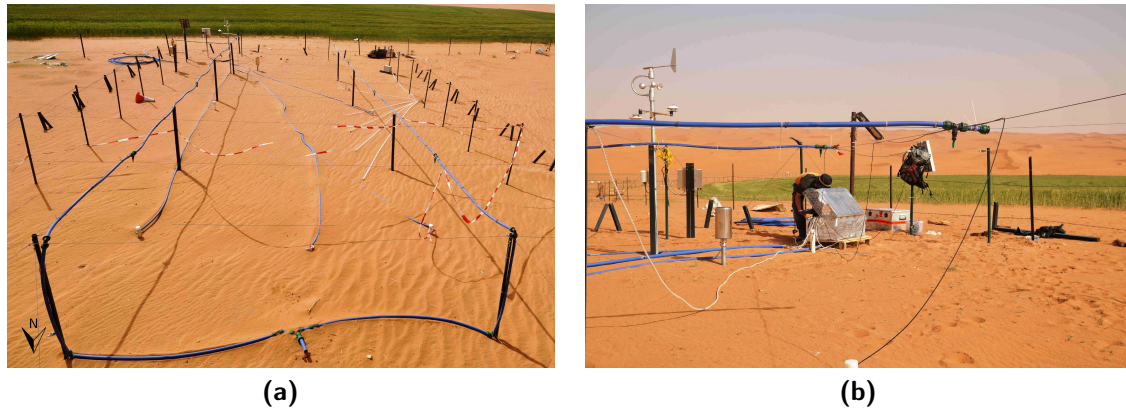


**Fig. 5.6.:** Overview to the test field on the Al-Adel farm (a) with base station for measure- and logger technique in the box, the weather station, solar panels and installed TDR-sensor heads (b).

The basic idea was to cover the sensors with a material which has similar dielectric properties like the desert sand. The material should be moisturized homogeneously to receive a specific travel time.

The focus was to deduce a calibration function. That should allow to get an integral moisture content along the whole sensor and a spatial resolution. The following subsections explain the approach to the experiment.

### 5.3.1. Analyses of Field- and Laboratory Sand Dielectrics

The selected fine grained sand was analyzed at the Institute of functional interfaces at the Karlsruhe Institute of Technology. As a reference five samples from Saudi Arabia were used.

The dielectric constant ( $K_a$ ) of the sand was measured with a copper made coaxial construction. It consists of a small conical pulse inductor and a hollow cylinder as the circumferential outer conductor. Fig. 5.7 illustrates that instrument.

The  $K_a$  was deduced by measuring the different sand inside the cylinder. The TDR signal was induced with a Hewlett Packard 8712C RF Network Analyzer via the central cone (fig. 5.7b). With the help of reference measures in air and water the  $K_a$  could be calculated by the different travel times (chapter 4.1).

For the sands the  $K_a$  was measured with a frequency that ranged from 200 MHz to 1100 MHz. The average of the five measured  $K_a$  for Saudi sand was appointed to 2.7 at a temperature of 22.2 °C (tab. 3.1).

The apparent dielectric constant of laboratory sand was calculated to 2.24.

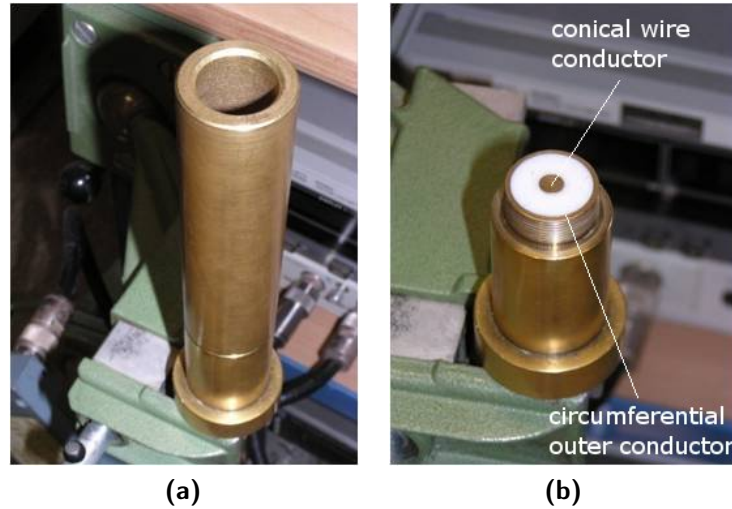


**Fig. 5.7.:**  $K_a$  measuring cylinder construction (a) with a coaxial structure (b).

**Tab. 3.1.:**  $K_a$  of desert sand.

sample	soil depth [cm]	$K_a$
1	20	2.77
2	40	2.64
3	60	2.62
4	80	2.80
5	80	2.70
average		2.71
lab sand		2.24

It can be assumed that a calibration function for the laboratory sands should be also valid for the sands of the test field in Saudi Arabia.

### 5.3.2. Experimental Pretests

The challenge was to get a homogeneous moisturized sand in the laboratory. The calibration of the sensors was carried out in three attempts.

#### Moisturization with a Sprinkler from Top

In the first of these experiments the sensors were placed to a box and covered with the pre-analyzed sand. With several measurements it was checked that only the dielectric of the sand influenced the TDR signal. The surface was moisturized with a sprinkler. Three liter of tap water were used for wetting.

Afterwards the surface was covered with an impermeable plastic sheet. Three days after the TDR measurements, sand samples were taken with core cutters in regular distances. The sand was dried at 105°C in an oven and the volumetric water content was calculated (Rowell, 1997). The process was finished by drying all the sand to air dryness in large basins. That procedure was repeated four times, the only shifted factor was the amount of water.

Two major problems occurred. The first problem was the spatial distribution of water. The prediction of a homogeneous sand could not be reached with this method. Fig. 5.8 shows that as an example. While the water on the right side infiltrated just 2–4 cm, the infiltration process was much more intensive on the coin side. However, there was no special pattern for these fingering effects.

The second problem was the very time consuming process. Each wetting cycle took around four days. Consequently, the experiment was canceled to try an alternative.

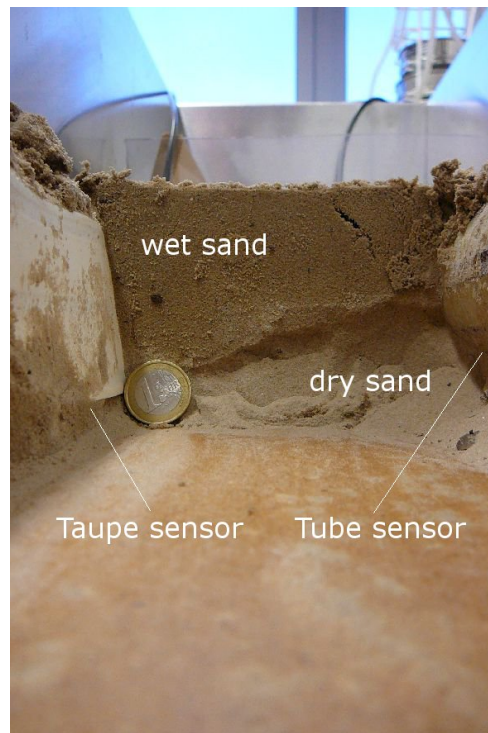


**Fig. 5.8.:** Irregular distribution of moisture three days after moisturization. Wet sand above and dry sand right to the coin.

### Moisturization in a Basin from the Bottom

Similar to the first calibration attempt the sensors were put horizontally to a box. However the setup was much more sophisticated. With a new box it was possible to

irrigate the sand from below. Air entrapments and fingering effects should be reduced in this way. The box was equipped with a water permeable double bottom and a filter fleece, which should avoid the trickling of sand into the hollow spacing. It could be assured, that the water table could reach the double bottom everywhere at the same moment.

Above the fleece the sensors were installed horizontally in the sand. Reference measures were taken with five self constructed and calibrated TDR short rod sensors which are described in chapter 5.3.3. The objective was to irrigate the sandbox until saturation. A subsequent drainage should let decrease the sand water content in the basin gradually. The short rod sensors measured the moisture content very fast and non destructive. The whole setup is displayed in fig. 5.9.

The experiment worked well until the water should drain. The mesh width of the filter fleece was chosen too wide. The sand ran through and plugged the drainage pipes. After having waited for three days the soil moisture content did not change and the experiment was aborted.

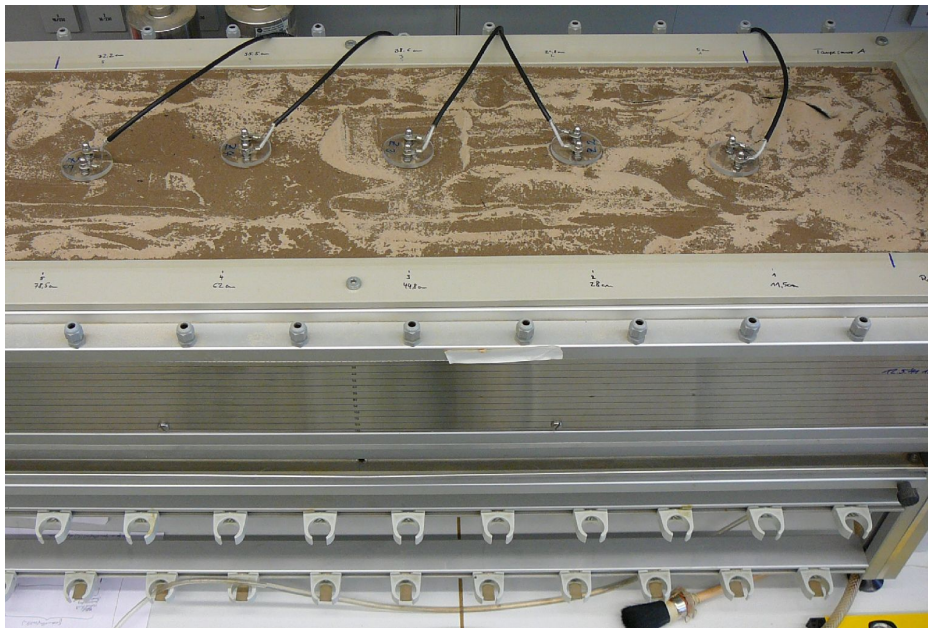


**Fig. 5.9.:** Finished setup of the second experiment with the additional five short rod TDR sensors during the irrigation process from the bottom, just before saturation.

### 5.3.3. Construction of own TDR Sensors

The concept for the second calibration pretest (chapter 5.3.2) included five independent short rod TDR sensors.

In contrast to Taupe- and tube sensor the short rod sensors are uncoated. Therefore it was possible to calibrate them with the equation of Topp et al. (1980), which is given on pg. 7.

The rods made of stainless steel are screwed to a disc of acrylic glass. The length of the probe rods is 7.5 cm. That corresponds to Dirksen (1999, pg. 32) who recommended a minimum size of at least five centimeters to get sufficient accuracy. The pins are connected to a 50  $\Omega$  Coax cable with a BNC plug (fig. 5.10).

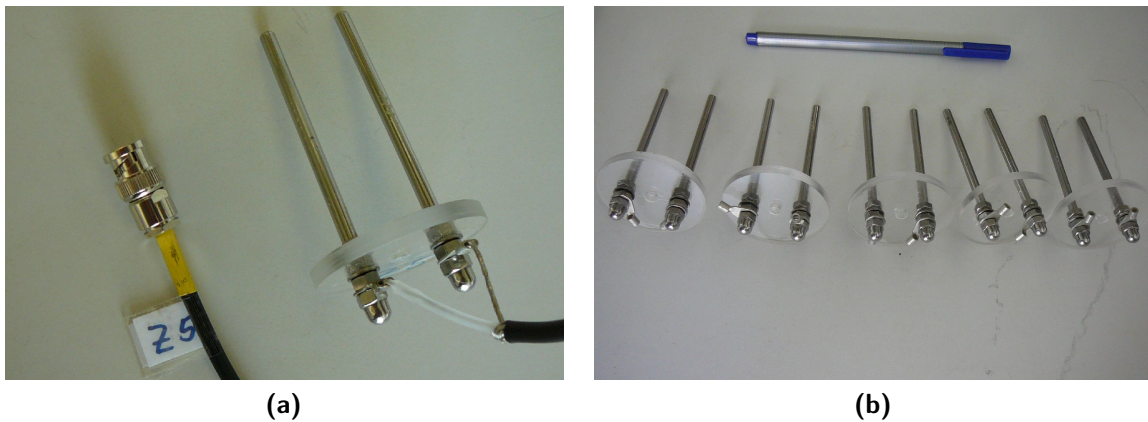


**Fig. 5.10.:** short rod sensors

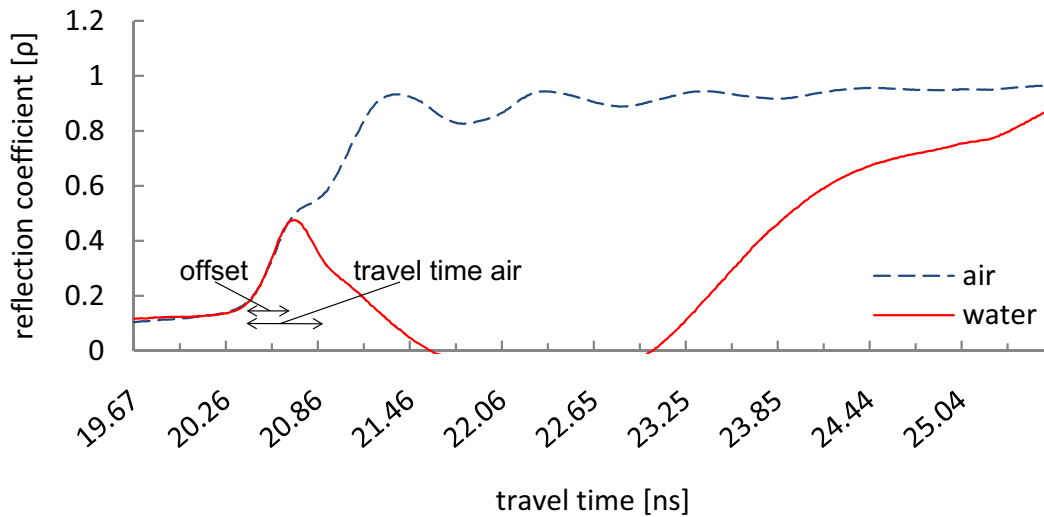
Next to the calibration a couple of sensor specifics have to be deduced using a self-made sensor. For this purpose they were measured in air and water to identify the travel time in air and the offset (chapter 4.2).

Fig. 5.11 shows these two measurements. The distance between “start travel time” and the spread of the air- and water signal defines the offset. It was identified as 0.248 ns. The travel time in air is 0.254 ns.

### 5.3.4. Calibration Setup for the Taupe and Tube Sensor

The first and second experiment attempt (chapter 5.3.2) have been realized under the assumption of same initial conditions i. e. soil bulk density. The only variable was the water content.

This third experiment was carried out under the assumption that soil bulk density is not the decisive reason to change the apparent dielectric constant ( $K_a$ ) of the air-



**Fig. 5.11.:** Travel time of sensor Z 5 between start and stop time, adjusted about the offset.

water-grain mixture. With a value of 1 air is by far closer to the  $K_a$  of the sand than water with a value of 80.

Taupe- and Tube sensor were similarly arranged to the previous experiment attempts. They were put horizontally to the box (fig. 5.12). However the sand was externally hand mixed with an specific amount of water, then it was filled to the box. The sand covered the sensors sufficiently. Subsequently TDR measures were executed for the two long rod sensors.

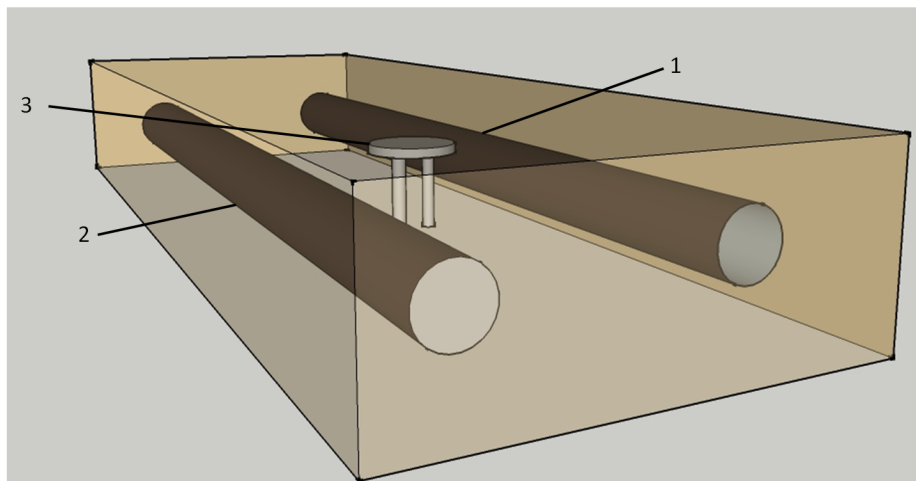


**Fig. 5.12.:** Calibration setup for the three sensors types: 1 and 2 – TDR field sensors Taupe and Tube, 3 – short rod TDR probe Z 5 in a sand filled box.

To monitor the sand moisture content the short rod sensor Z 5 was used. TDR measurements were taken at point P1–P5 along Taupe- and Tube sensor. Additionally,

one sand sample was taken for oven drying. The setup and the measure points are illustrated in fig. 5.13.

Afterwards, the sand volume was removed from the box. It was enriched with more water and put back to the box. This procedure was repeated in 20 individual cycles. The water amounts are given in appendix tab. A.1.

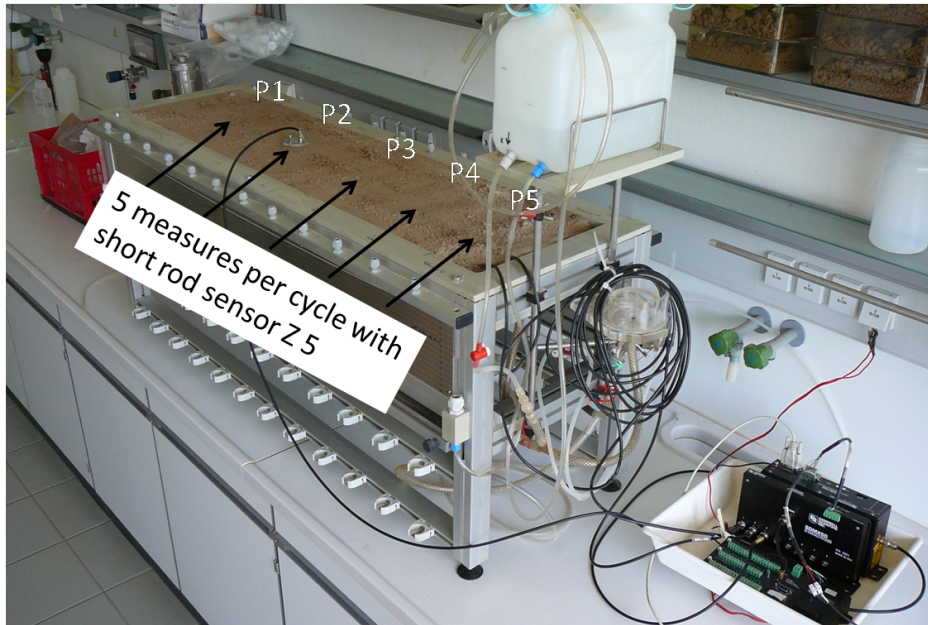


**Fig. 5.13.:** Sandbox for TDR measurements and measuring technology in the right bottom corner; measure points P1–P5 with sensor Z 5.

## 6. Results and Discussion

### 6.1. Climate and Weather Analyzes

#### 6.1.1. Results of TRMM Data Analyzes

The objective of TRMM data analyzes was to find the frequency and variability of precipitation events in the test field region. These analyzes show the general climatic reliability of the test field.

The chart in fig. 6.1 shows the mean amount of precipitation for single months between 1998 and 2008. It can be noticed that the sum of precipitation for these ten years are very low with around 90 mm. The diagram shows an irregular distribution of precipitation. The months June till October are dry. Between November and May are two maxima, one in December and the other in April.

The comparison between pixel five and all nine pixel show that the area around the test field is affected by low differences of amount and distribution of precipitation.

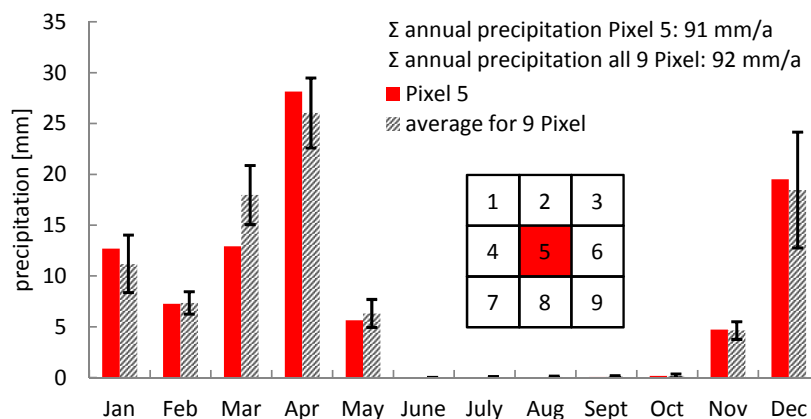


**Fig. 6.1.:** Distribution of precipitation for ten years: pixel five.

Therefore only pixel five was analyzed. In 146 days out of ten years precipitation was observed (fig. 6.2). The most frequent rain events consist of one millimeter. Events with four and more millimeter occur nine times per year on average.

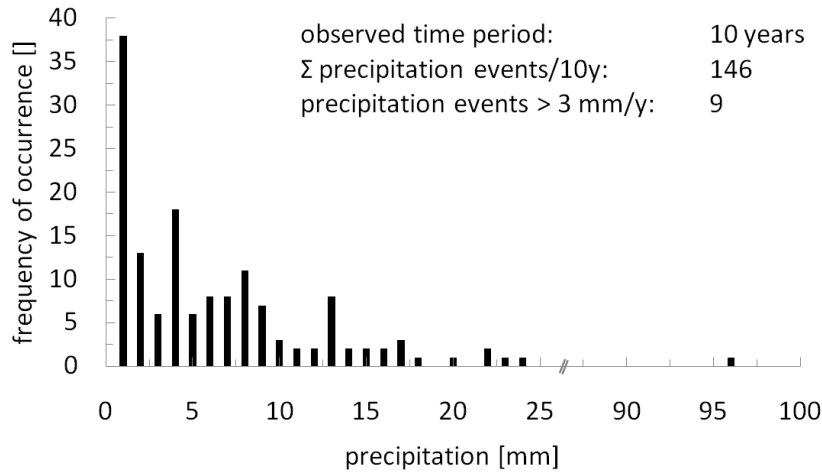


**Fig. 6.2.:** Frequency of occurrence of precipitation for a period of ten years.

### 6.1.2. Weather and Soil Temperature of the Test Field

This section gives an overview about weather conditions in the monitoring period. This is essential to understand infiltration processes which will be explained in the following sections.

Figure 6.3 on pg. 28 shows the air and soil temperature and the precipitation events for the observed time period between March 3rd, 2011 and July 7th, 2011. The data was measured with the climate station on the test field (chapter 5.2). The soil temperature in this figure is derived from the sensors which are part of the diagonal Taupe TDR system. Names and depths of the temperature sensors are given in table 2.1.

The air temperature shows a seasonal trend with low values in spring and high values in summer.

The four precipitation events over one millimeter take place around March 10th, the mid and end of April and the end of May. The first one is a cluster which is distributed about several days with lower and higher single events.

The rainfall events in April are very low with less than 3 mm water amount.

The last one is the most abundant single event with six and a half millimeter. The air temperature is affected by these rainfalls. The air humidity correlates negatively with the temperature—as expected and also the sand in the upper layers cools down. These slightly delayed short term changes can clearly be noticed from the top soil temperature sensor T1 in half a meter depth. Generally it can be assumed that except to March, 31st precipitation had an influence to the temperature. The other way around measuring errors of the precipitation transmitter can be excluded, while presuming a correctly working air thermometer.

Greater depths only consist of smooth long term temperature changes. In circa two meter depth daily fluctuations are no more noticeable. The deeper the sand the more delayed it reacts to atmospheric changes. The long term range also becomes smaller. Due to these reasons T5 and T6 run opposite to the atmospheric temperature. Data of T3 only exist sporadically. There are much missing data related to a cable break.

## 6.2. Calibration Results

### 6.2.1. Soil Moisture Content with TDR Short Rod Sensor Z 5

Fig. 6.4 shows the soil moisture content of the 20 wetting cycles of chapter 5.3.4. The graph *moisturization amount* shows the theoretical volumetric water content. It is derived by calculating the added water to the total sand volume in the box. The *thermogravimetric determined* data results from sand samples, which were taken from the sandbox in the laboratory. The *Topp's equation* graph was derived with equation 4.8 and the single offset corrected travel times in air and sand (chapter 5.3.3). The graph of *Cal.fct.*<sup>3</sup> is a Topp alternative 3rd degree polynomial function, which is adapted to thermogravimetric determined data (equation 6.1).

$$\Theta_{vol}\% = -13.93 + 6.9501 \cdot K_a - 0.5494 \cdot K_a^2 + 0.0173 \cdot K_a^3 \quad (6.1)$$

The current measured soil moisture passes in each cycle little above the theoretically expected value. In the first ten cycles they differ round 16 percent. In contrast the difference in the second ten cycles have a deviation of three percent on average. Both graphs provide a satisfying range for the calibration of the short rod sensors. It is an indicator that the adjusted offset and travel time in air must be chosen correctly. Nevertheless it is a *universal* calibration function and passes the other graphs a bit divergent. In the range between first and tenth moisturization cycle the *Topp's equation* graph slightly underestimates soil moisture while in the cycles eleven and higher it overestimates it.

On the basis of the proven adjustments the 3rd degree polynomial equation adapts the thermogravimetric determined data best—as expected. Therefore it was chosen to calculate soil moisture content for all five measure points in the sand box experiment.

The homogeneity of the distribution of soil moisture content can be derived from fig. 6.5. The average result for measure points P1 till P5 (chapter 5.3.4, fig. 5.13) and their standard deviation is shown in the chart. In the first four cycles the measures

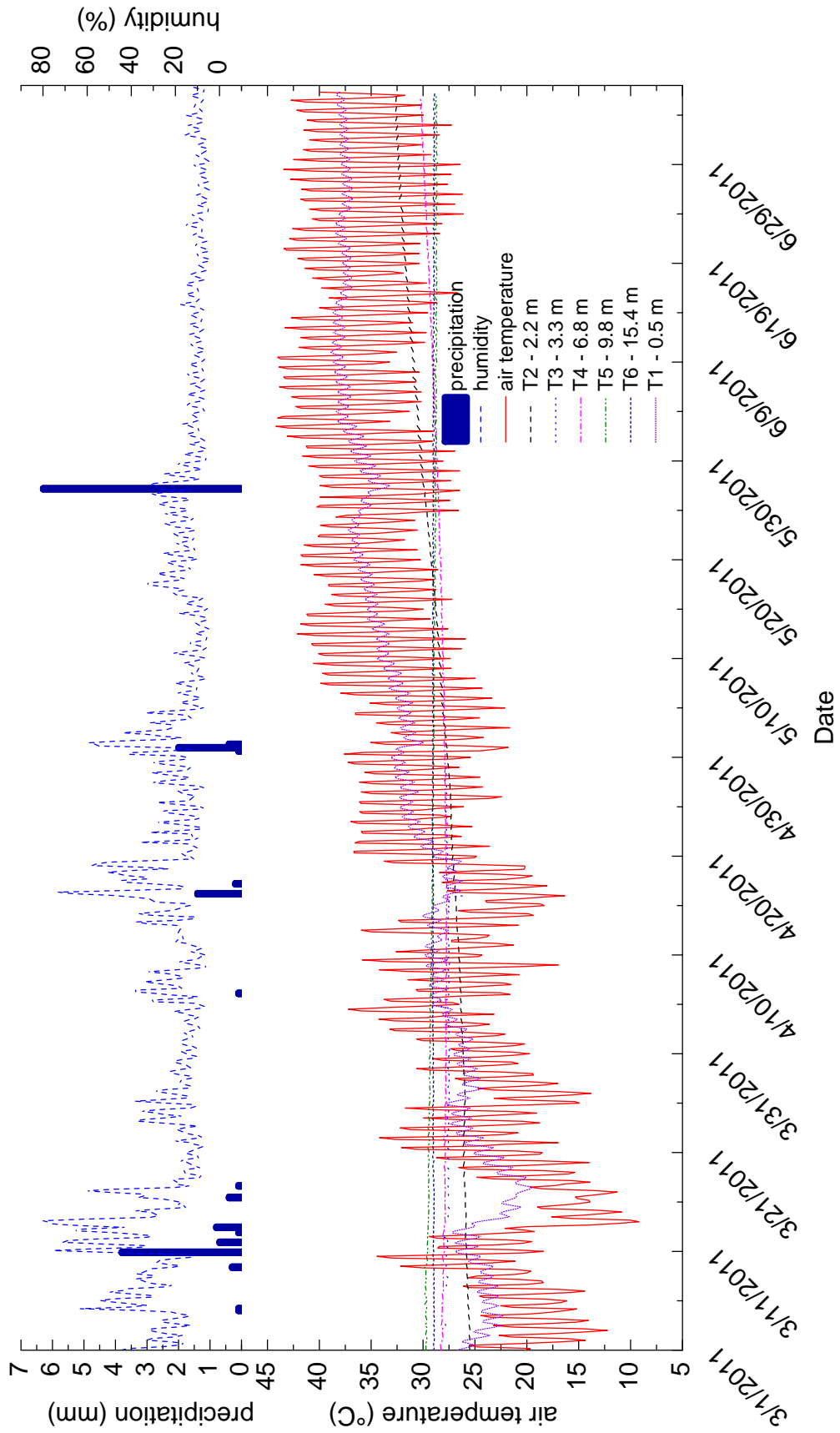
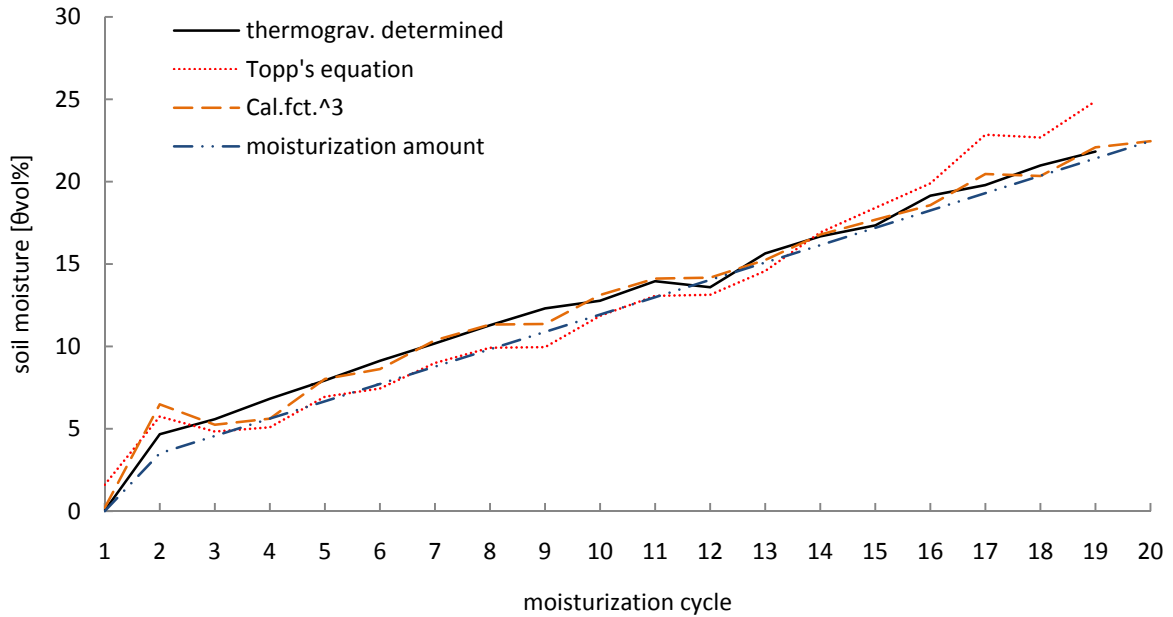


Fig. 6.3.: Air temperature and precipitation from test field climate station; Soil temperature T1–T6.



**Fig. 6.4.:** Measurements of sand moisture content and adjusted calibration functions.

differ in between 5 vol.%. The rest of the values differ less. The reason for these differences is probably an insufficient mixing. Dry sand is harder to mix homogeneously than moist sand, thus these differences seem to be obvious. The single and average VWC from sensor Z 5 can be looked up in tab. A.3 of the appendix.

The correctly calibrated short rod sensor Z 5 makes it possible to allocate a moisture content to specific length marks on Taupe- and Tube sensor.

### 6.2.2. Integral Soil Moisture Content with Taupe and Tube Sensor

The challenge of this section is to provide calibration functions of the Taupe and Tube sensor. This work step gives a relation between  $K_a$  and soil moisture content. Via the equation it will be possible to calculate an *integral* VWC from travel time for the whole sensor.

Taupe- and Tube sensor were similarly calibrated to short rod sensor Z 5. The travel time in air and the offset is given in tab. 2.1.

**Tab. 2.1.:** Constant travel times for Taupe- and Tube sensor, the travel time in air is offset corrected.

	travel time air [ns]	offset [ns]
Taupe	3.737	0.393
Tube	4.029	0.314

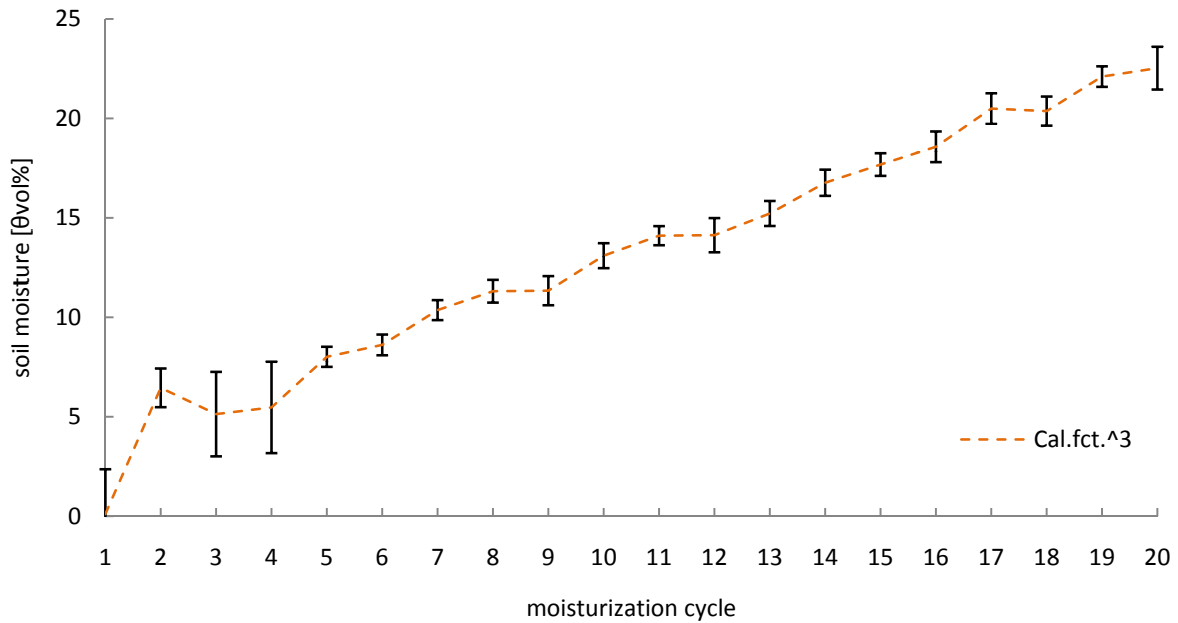


**Fig. 6.5.:** Average results derived with 3rd degree polynomial function for P1–P5 and their standard deviation.

To calibrate the sensors the thermogravimetric derived results were used.

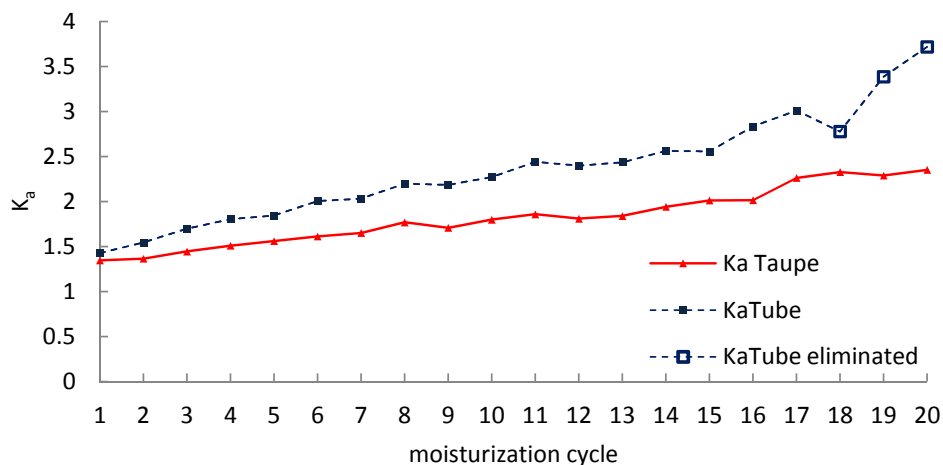


**Fig. 6.6.:**  $K_a$  analysis of Taupe- and Tube sensor.

The  $K_a$  of Taupe- and Tube sensor were analyzed ahead the calibration. Fig. 6.6 shows the slightly increasing  $K_a$  for both sensors. The slope of Taupes  $K_a$  is a bit shallower. That is respected to the insulating material that makes the sensor less sensitive to dielectric changes (Scheuermann et al., 2002, pg. 189).

However the last three of the tube values do not fit to the trend of the previous ones. The reason for the low first value might be an air entrapment at the end of the sensor. The hint to that assumption can be found in the course of the signal

(fig. 6.10). The signals total reflection occurs too early and looks irregular—maybe because an excavation. The significant higher value of the last two points could not be cleared completely. Indeed, the relation of soil moisture content and  $K_a$  is not linear. Nevertheless, tests showed that the values are still too high. For the calibration these three values were not respected.

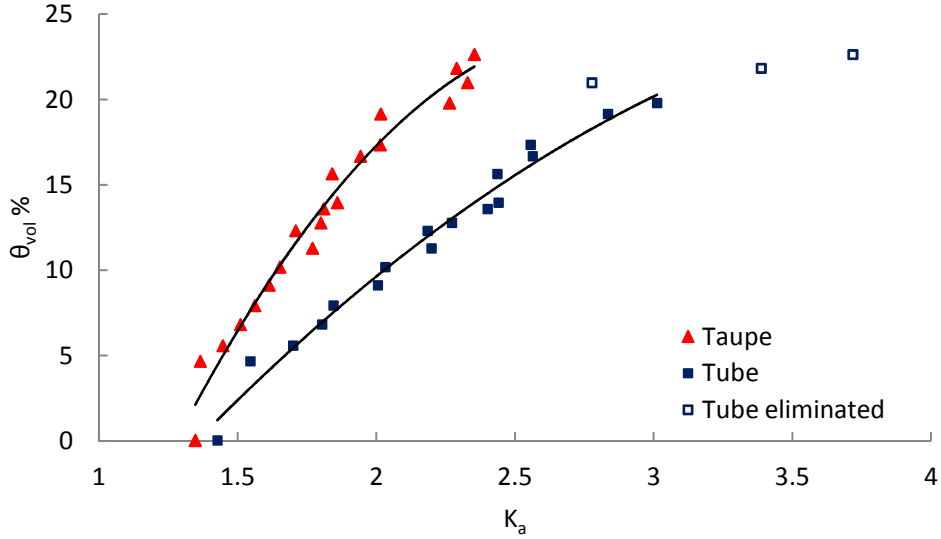


**Fig. 6.7.:** Calibration for Taupe- and Tube sensor.

For the calibration the VWC was plotted in dependency to  $K_a$  (fig. 6.7). The lower sensitivity of the Taupe sensor is also reflected in this chart. The not respected data points are displayed hollow. The calibration functions are shown in equation 6.2 for Taupe- and equation 6.3 for Tube sensor.

$$\Theta_{vol}\% = -8.8317K_a^2 + 52.284K_a - 52.08 \quad (6.2)$$

$$\Theta_{vol}\% = -3.2823K_a^2 + 26.589K_a - 30.253 \quad (6.3)$$

These equations were used for measurements in the laboratory sand box and as well for the field measures. To check the equations,  $K_a$  was applied on them. The results are displayed in fig. 6.8. It can be noticed that the results fit well to each other. The differences of the calculated to the thermogravimetrically derived values are located between 2 vol% at the “dry” end and less than 1 vol% in the rest of the charts.

It can be assumed that Taupe- and Tube sensor are able to measure the integral soil moisture content sufficiently.

The corresponding variables which were used for calculation, as well as the VWCs are given in tab. A.4 for the Taupe sensor and tab. A.5, for the tube sensor.

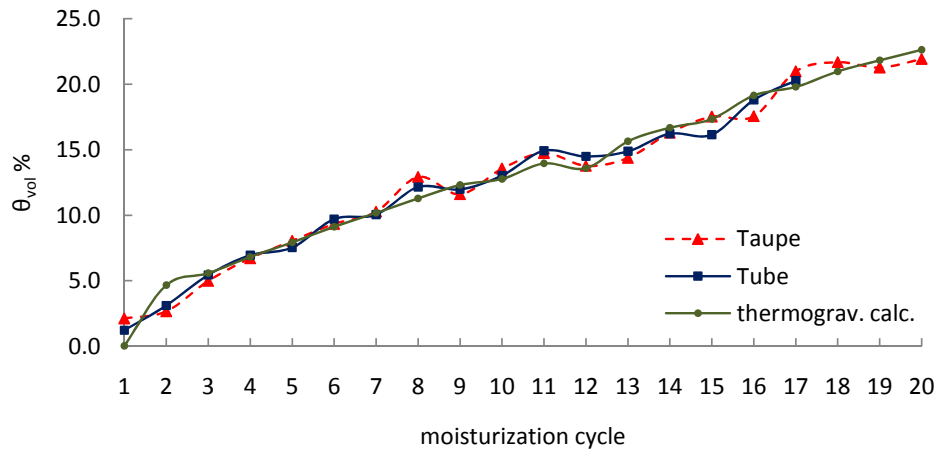


**Fig. 6.8.:** Calculation of volumetric water content with the calibration functions 6.2 and 6.3.

### 6.2.3. Spatial Distribution of Soil Water Content

One main objective of this work was to determine the *spatial* distribution of water content. With the help of the integral VWC (chapter 6.2.2) and the reflection coefficient ( $\rho$ ) it was possible to receive results about that issue.

The explanation of TDR signals is given in chapter 4.2.

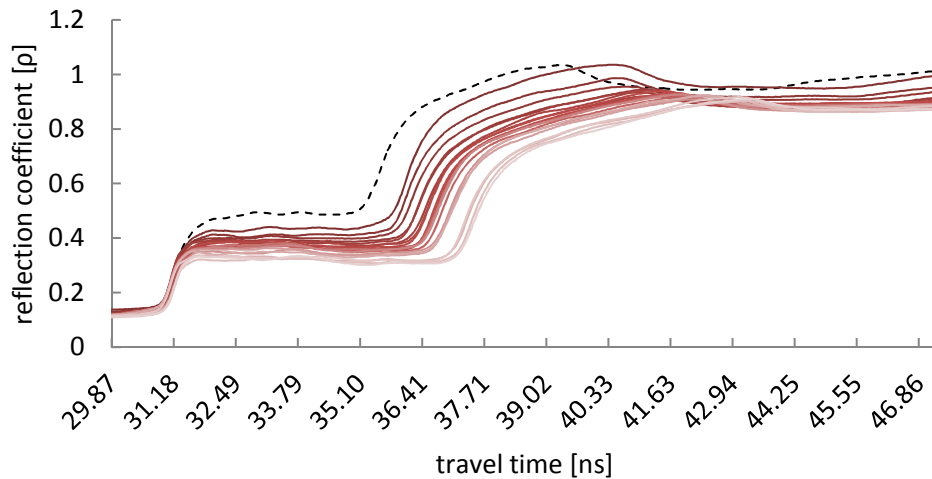


**Fig. 6.9.:** Taupe: 20 TDR signals from sandbox experiment II plus the signal in air: The brighter the color the longer the signal, the moister the sand. In black: TDR signal in air.

The charts in fig. 6.9 and 6.10 show the TDR signals for the 20 different measurements. Additionally the signals in air are given as a reference for both sensors. Each measured

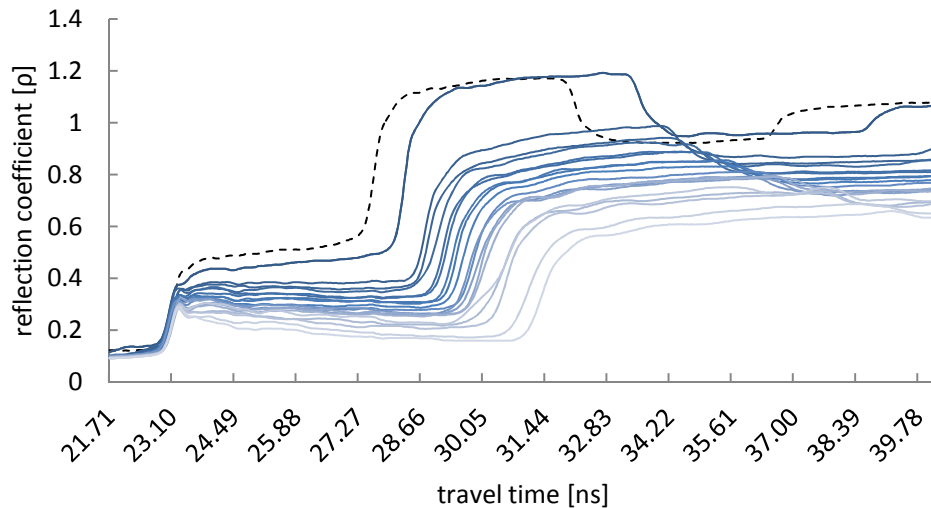


**Fig. 6.10.:** Tube: 20 TDR signals from sandbox experiment II plus the signal in air: The brighter the color the longer the signal, the moister the sand. In black: TDR signal in air.

curve consists of 600 data points. This setting was defined before the measures. They are important to receive exact travel times but to get an accurate spatial resolution as well. More points would be possible but they also need more storage space and become unhandy for analyses.

The length of the considered time frame was chosen generously too long. This avoids a too early cut off of the signal during the experiment. Comparing both data sets the steeper increase of the Taupe calibration function can be reconstructed. The length of those signals does not grow by far as much as the tubes signal. Reasons are the insulation of the steel rods which reduce the increase of the apparent dielectric constant ( $K_a$ ).

An important challenge of this chapter is the progression of the first reflection representing “plateau” part (chapter 4.2). The “air” signal of Taupe shows two little, convex waves. They reoccur as well in the driest sand measurements. With an increasing soil moisture content this influence decreases. In various tests with the free-standing sensor without sleeve and tube this anomaly was not observed, therefore the reason seems to be the fixation with cable straps to the HDPE-tube.

The second observation is a slightly decreasing trend of the reflection coefficient to the end of the sensor. This trend becomes stronger with the increasing moisture content. It is much stronger in the Tube-, than in the Taupe TDR signals. It is respected to the electro conductivity (EC) of the tap water that attenuates the reflection coefficient.

However the sand mixing method and the results from point measurements with sensor Z5 conclude that the distribution of water was roughly homogeneous. This result was transferred to the TDR-signal via detrending with linear, signal individual functions. The distinctive start and end slope were cut off.

The result of this work step is shown in fig. 6.11 and 6.12. The abscissa was redefined to dimensionless measure points respected to shifting operations to reach standardized start points. The first point of each chart has still the same value as before detrending.

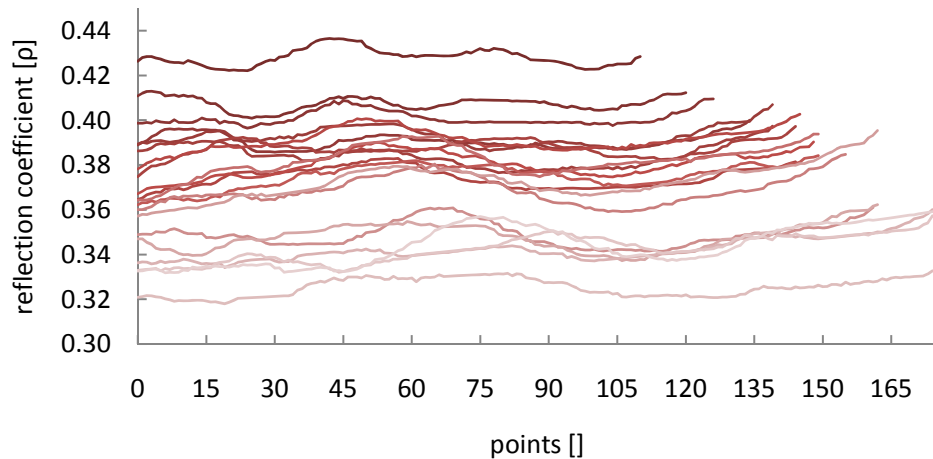


**Fig. 6.11.:** Taupe: 20 detrended plateau parts of the original TDR signals, arrangement of signals analog to fig. 6.9.

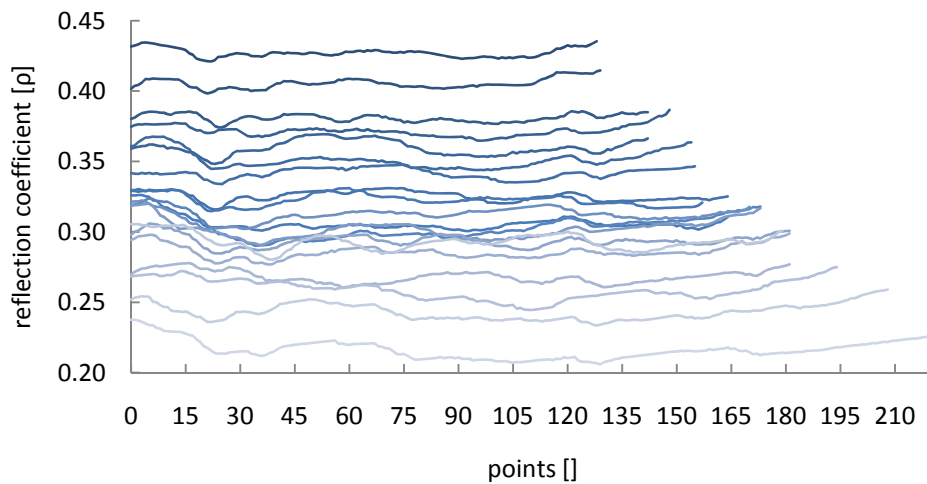


**Fig. 6.12.:** Tube: 20 detrended plateau parts of the original TDR signals, arrangement of signals analog to fig. 6.9.

To compare moisture contents from different measurements at a specific length point of the sensor it has to be realized that this point “moves” in dependence to

the surrounding moisture. This expansion problem was solved by downscaling. The procedure is exemplified for the 80 cm Taupe sensor in fig. 6.13.

Each of the 20 signals got its own *decimal* 80 cm scale. Respected to the increasing amount of measure points of the “plateau” part the number of the scale points was different for each signal.

In the next step decimal scales were changed to *integer* scales, therefore equal scale values appeared. In the third and last step the signal values of equal scale values were taken to an average. As a result all 20 signals had one centimeter resolved values. The same procedure was carried out for the 100 cm long Tube sensor.

scale 1	0	0.5	1	1.5	2	2.5	...	...	80	Decimal
signal values	value 1	value 2	value 3	value 4	value 5	value 6	...	...	value n	
scale 1	0	0	1	1	2	2	...	...	80	Integer
signal values	value 1	value 2	value 3	value 4	value 5	value 6	...	...	value n	
scale 1	0		1		2		...	...	80	Integer
signal values	average of value 1 and value 2		average of value 3 and value 4		average of value 5 and value 6		...	...	average value n	

**Fig. 6.13.:** System of shortening the different long TDR-signals.

From the detrended and shortened signals the reflection coefficients were averaged to get  $\bar{\rho}$ . The calibration functions were calculated from these results and the thermogravimetric determined moisture contents. The corresponding diagram is given in fig. 6.14. For the Taupe sensor the relation water content to  $\rho$  is slightly polynomial (equation 6.4), while that of the Tube sensor is nearly linear (equation 6.5).

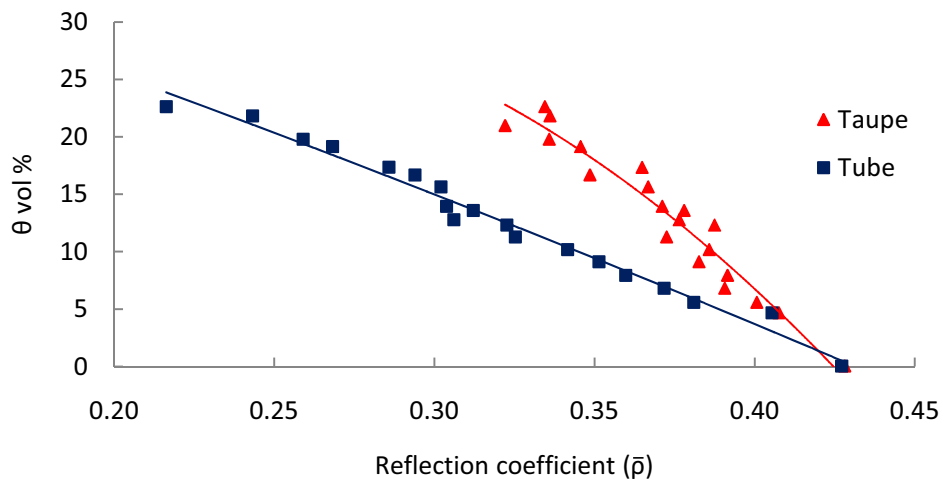


**Fig. 6.14.:** Calibration functions from Taupe- and Tube sensor for the reflection coefficient.

$$\Theta_{vol}\% = -670.25\rho^2 + 278.01\rho + 2.7906 \quad (6.4)$$

$$\Theta_{vol}\% = -36.731\rho^2 - 87.166\rho + 44.441 \quad (6.5)$$

The reflection coefficients ( $\rho$ ) were applied to these equations. The result is the calculated spatial distribution of sand moisture content for the moisturization cycles. This is shown in fig. 6.15 for Taupe- and fig. 6.16 for Tube sensor. The color ramp is similar to the original signals from fig. 6.9 and 6.10. The moister the sand the brighter the color.

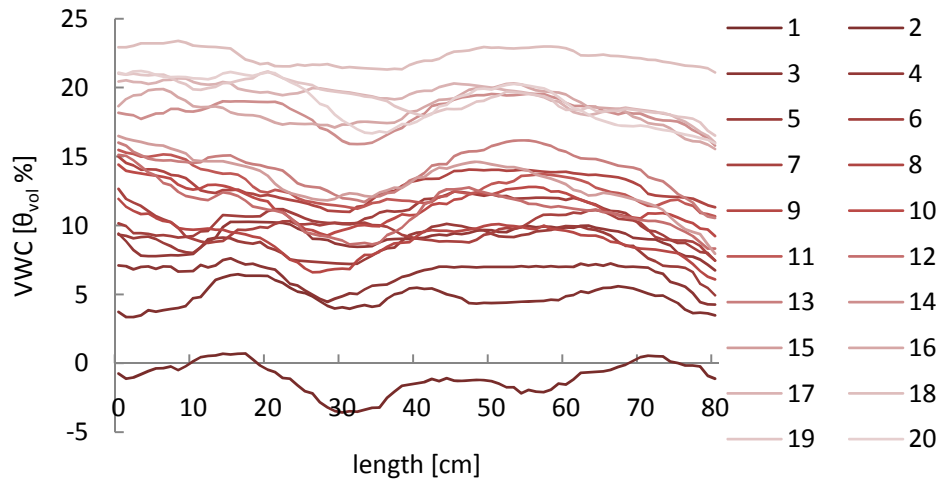


**Fig. 6.15.:** Taupe: Spatial distribution of sand moisture content of 20 moisturization cycles.

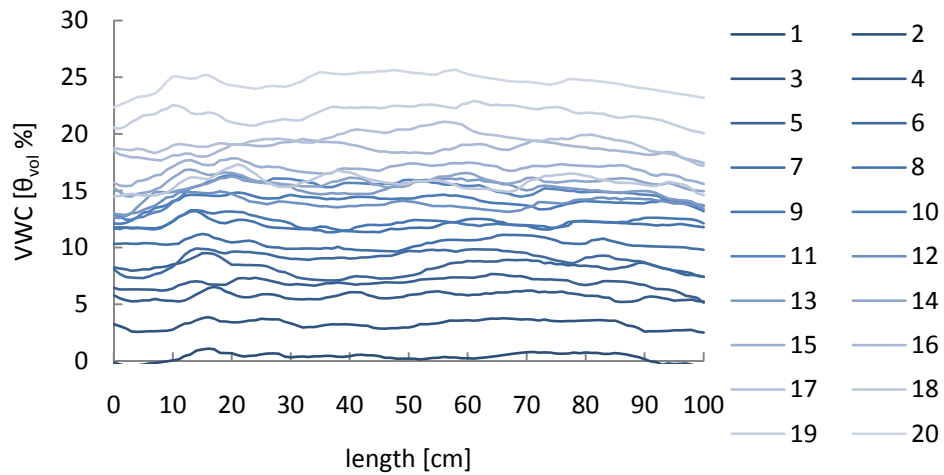


**Fig. 6.16.:** Tube: Spatial distribution of sand moisture content of 20 moisturization cycles.

The different moisture contents are clearly exposed in both figures. However the range of the Taupe VWC varies much more than the results of the Tube sensor. The most obvious explanation is the mechanic combination of the HDPE-tube and the flat ribbon TDR cable. The measurements in air show two noticeable waves which are again in the results.

It can be resumed that these waves should be removed by mathematical adjustment. The results would be more homogeneous. Nevertheless the construction is the reason for the problem, therefore it should be changed. Furthermore the first measurement is on an average below 0 vol% soil moisture content. Off course, this is not possible and shows uncertainties of the calibration.

Although the tube sensor is mechanically much better designed, the results also consist of obvious, but smaller reoccurring characteristics. They appear as peaks between ten and twenty centimeter and as a gentle decrease towards the end. Especially this downward movement could be solved by a more sophisticated detrending algorithm.

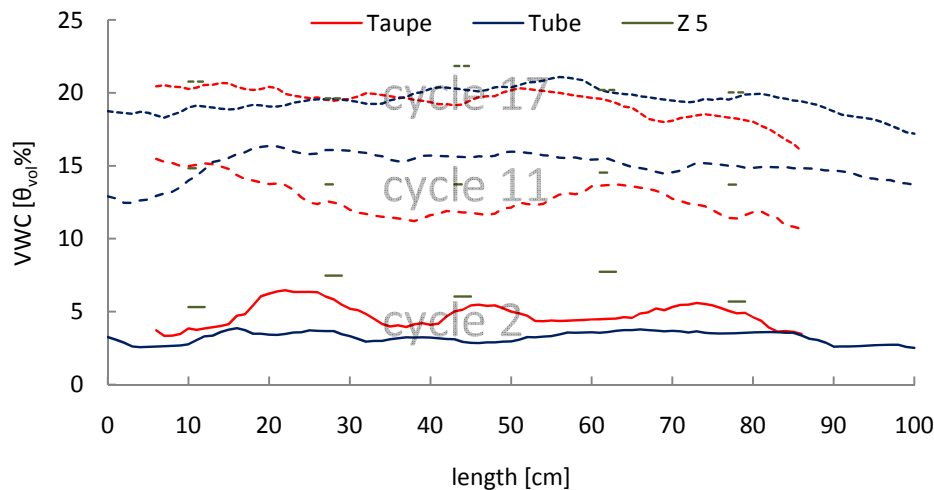


**Fig. 6.17.:** Comparison of exemplary moisturization cycles 2, 11 and 17.

In fig. 6.17 the measurements of moisturization cycle 2, 11 and 17 are compared in true scale. In cycle two Z5 has markedly higher results than Taupe and Tube. In cycle 11 both long sensors are better adapted to Z5's measurements whereas Tube overestimates and Taupe underestimates the moisture almost about the total length of the sensor. Cycle 17 gives the best accordance. The deviation is about half the one than in cycle 2 and 11. However it can be concluded that the best results can be found between 10 and 20 vol% moisture content.

### 6.3. Integral Soil Moisture of TDR Field Measurements

The following considerations are based on data from March till July 2011. With respect to technical problems only the six vertical sensors are used to estimate soil moisture content. The Taupe sensors are not considered. The upper one (T1) is disabled because of a mechanical disruption between COAX Cable and BNC-plug. The deeper one (T4) is surrounded by a steel casing (chapter 5.2).

The ten signals in fig. 6.18 show the original TDR-signals which were measured in the field. The time gaps between are equidistant. The relevant time interval is located between the “start” and “end” marker. They are examples of all 767 signals between March and July 2011.

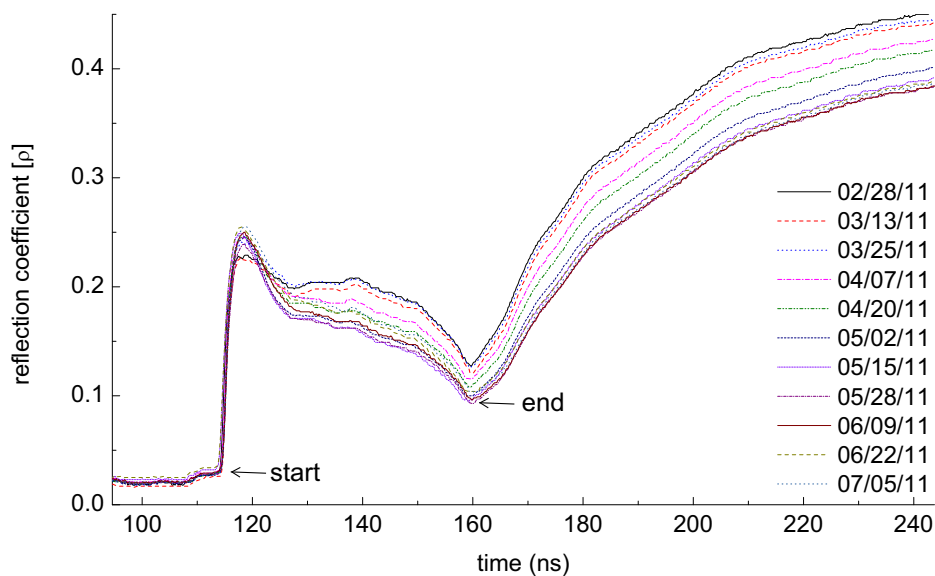


**Fig. 6.18.:** Ten representative TDR signals of sensor V3 between March and July.

For the calculation of the integral VWC of the six Tube sensors the travel time in air was used (Tab. 2.1). The laboratory determined values for the short sensor versions were extrapolated to the physical lengths of the field sensors. The related data are attached in tab. A.6. The soil moisture was calculated with the Taupe software (pk tools, 2006) and the calibration function from equation 6.3.

Fig. 6.19 shows the calculated *integral* VWC from all 767 measurements between March and July. The individual curves proceed homogeneously on different high VWC levels. The range of about  $\pm 5\%$  is the current uncertainty of the calculation. Therefore V1 shows  $\approx 5\%$  VWC at the beginning of March, while V6 shows between 13% and 14% at the same moment. The reason might be a systematic error, maybe

due to a mistake in the physical measured lengths or an erroneous calculated travel time in air.

It seems to be unrealistic that these high differences appear homogeneously just seven meters away from the neighbor sensor.

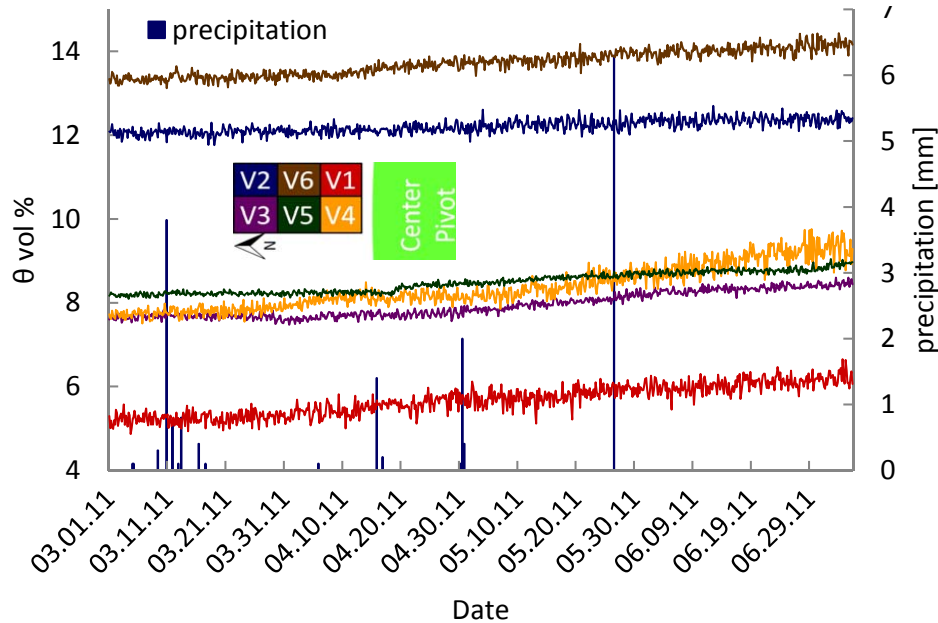


**Fig. 6.19.:** Integral VWC from March till July for the vertical Taupe sensors V1 – V6. The length of the sensors is given in tab. 2.2. The ground plan of the test field positions the signals.

Another noticeable property of fig. 6.19 are the marginal differences of the VWC over the whole time segment. The least differences between start and end of the observed period gives V2 with round 0.5 %, sensor V4 varies most with 1.5 %. The precipitation events obviously do not affect the VWC. Because of the long sensors and the less water amounts this result was expected.

Precisely *because* of this “insensibility” the long term slightly *increasing* moisture values attract attention and need to be challenged. This slight effect can be observed for virtually all sensors. The sensors V1 and V4 are closest to it and consist of the highest changes. The VWC of V3 which is farthest away from the center pivot increases least (fig. 6.21). An imaginable possibility seems to be the lateral influence of the center pivot next to the test field. In that case the soil moisture should distributed differently among the sensors. With increasing distance to the center pivot the soil moisture should start to increase in deeper levels (fig. 6.20).

Unfortunately there are no data available about irrigation on the center pivot therefore this proposal cannot be examined in this way.

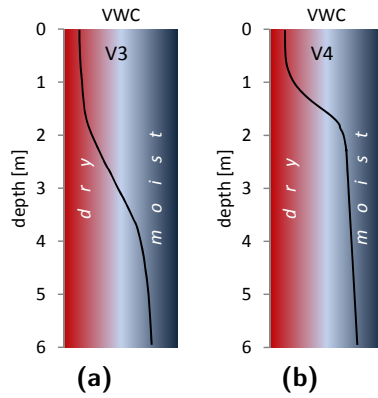


**Fig. 6.20.:** Assumed distribution of soil moisture content along the sensor. The distance of Sensor V3 (a) to the center pivot is round 30 m. The distance of V4 (b) to the center pivot is round 15 m.

Whether the soil moisture is located near ground surface or deeper sand layers cannot be detected in this methodical context. Indeed the *spatial* analyzes of soil moisture in the next section shall give an answer to this question.

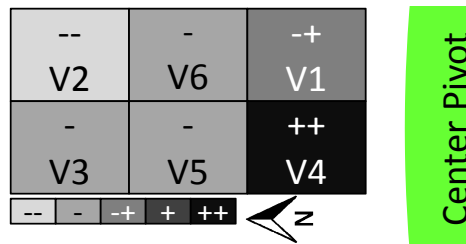


**Fig. 6.21.:** Ground plan of the test field: Increase of soil moisture content from March – July; ++ high differences, -- least differences.

## 6.4. Analysis of Measured Reflection Coefficients in a Spatial Context

As well as the travel time the reflection coefficient ( $\rho$ ) is a function of soil moisture content. The laboratory experiment (chapter 6.2.3) showed how  $\rho$  can be used to estimate water content. In this chapter the raw, unmodified signals are considered as a basis for further modeling.

The presented analyses were figured out for sensor V3. Just like V2 this is farthest to the center pivot with round 30 m. It is situated on the north western corner of the test field (fig. 5.5 and 6.21). With 6.30 m it is the third longest Tube sensor on the site.

Fig. 6.22 shows four TDR-signals of sensor V3 at marked dates. These are the signals with the most extreme  $\rho$  values in the whole monitoring period.

Chosen before and after the distinctive rainfall events in March and May they show short term amplitude changes. Likewise noticeable is the longterm decrease between the two measuring couples.

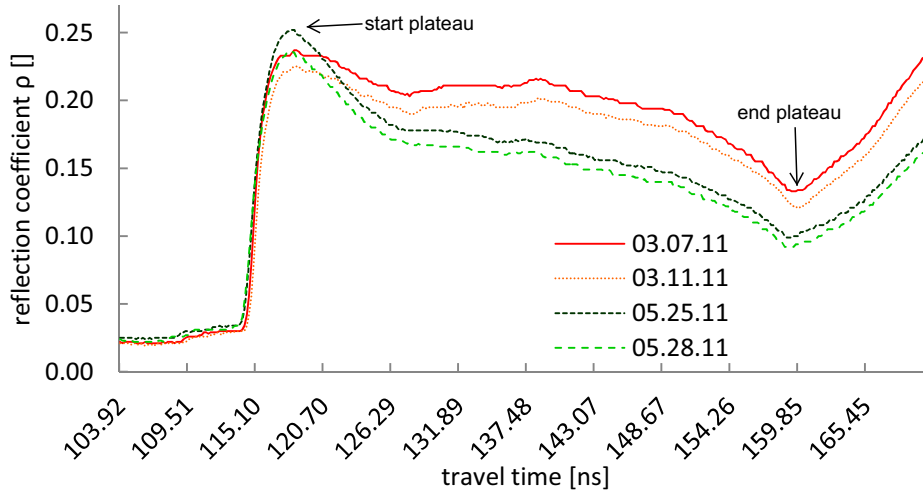


**Fig. 6.22.:** TDR-signals from sensor V3 at marked dates, before and after the most abundant precipitation events.

It is obvious that the lengths of the signals do not differ very much. That is reflected in the integral VWC which was presented in chapter 6.3. Indeed, the reflection coefficient is much more variable. The signals *after* the precipitation are in both cases below the older ones, what can be attributed to a general higher soil moisture content.

A more revealed view to that problem is offered by fig. 6.23. In contrast to the four signals of fig. 6.22 *all* measurements are included to this consideration.

The start and end of the signals were cut off. Afterwards the reflection coefficient of the plateau section was averaged ( $\bar{\rho}$ ). The precipitation is given as well and clearly identifies the significant decrease of the TDR signals as a change of soil moisture.

Indeed the signal decreases as well from the mid of March till the beginning of May but *without remarkable measured rain*. As long as the the signal decreases in this time, there is also a high  $\bar{\rho}$  jitter on it. A closer look to an exemplary high resolved period from March 29th till March 31st identifies this as daily fluctuations (fig. 6.24). Around four o'clock in the afternoon the jitter reaches its maximum while it is least between midnight and four o'clock in the morning.

From depart of May 10th, 2011 the jitter, as well as the long term decrease turns to the opposite. Only the rain event at the end of May disrupts the continuous drying

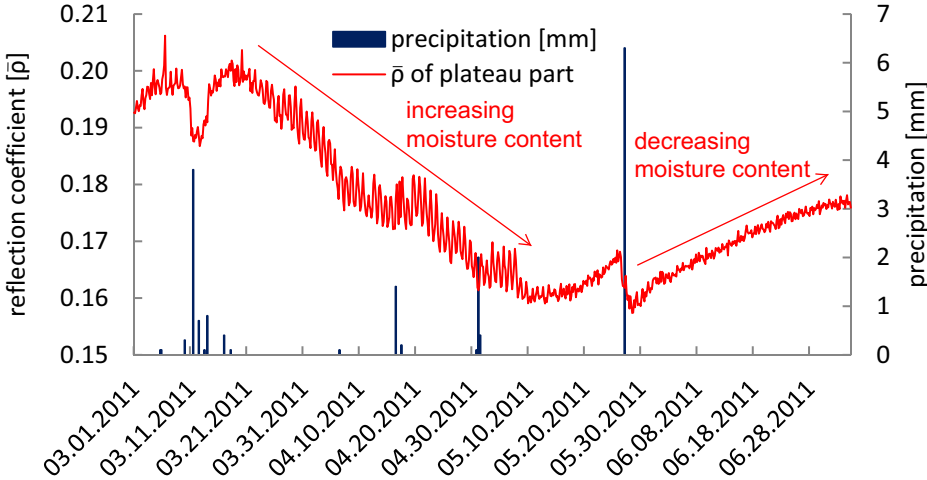


Fig. 6.23.: Average of reflection coefficient in the plateau period of a TDR signal.

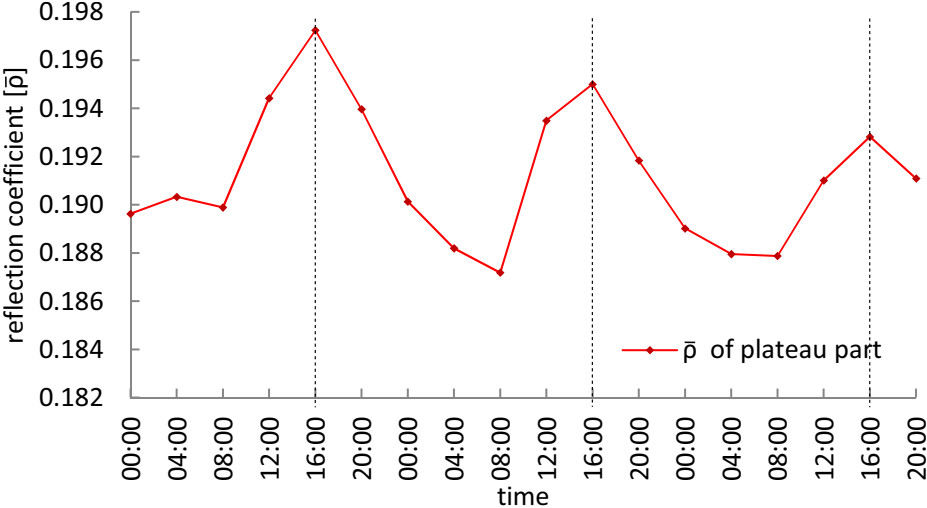
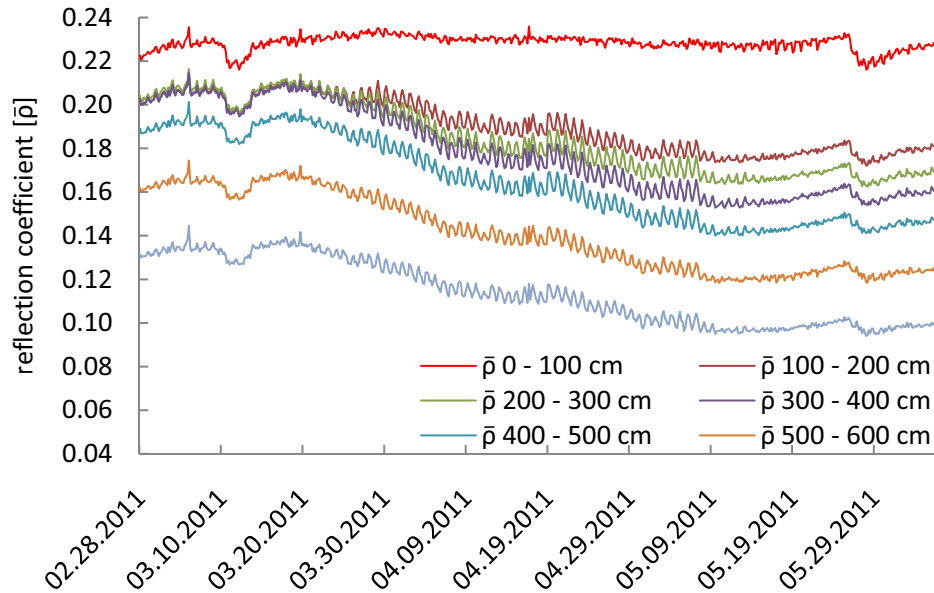


Fig. 6.24.: Daily fluctuations of the averaged reflection coefficient from March, 29th – March, 31st.

process and prolongates it for round 14 days. The reason for the phenomenon could not be clarified finally. Electromagnetic changes supplied by well pumps or hydraulic short term changes might be possible. Also atmospheric influences to the measuring technique might contribute the jitter.



**Fig. 6.25.:** Average of reflection coefficients for one meter sections of the TDR signal plateau.

In fig. 6.25 the plateau part of the TDR signal is analyzed still more detailed. Therefore it is divided into six one-meter- and one 30 cm section, according to its physical length of 6.30 m. These individual sections were averaged again. Virtually all depth sections show the pattern of fig. 6.23. Surprisingly only the first meter (red) shows the current rainfall events, the longterm moisture decrease *between* is totally absent.

## 6.5. Modeling Soil Moisture Contents

The laboratory experiments from chapter 6.2.3 showed that TDR signals from the Tube sensor are attenuated by the EC of tap water. Due to the design of the experiments the soil moisture was always homogeneous dispensed. Therefore the influence was linear and consequently the detrending function as well.

In contrast the field measured signals in fig. 6.22 are obviously not homogeneous. It can be seen, that the left (surface nearer) part is drier, while the right (deeper) part is moister. Accordingly a linear detrending would not sufficiently cover these conditions.

Therefore a slightly decreasing 2nd degree polynomial function (equation 6.6) was chosen to detrend the the whole set of signals.

$$\rho_{detrended} = -2.50 \cdot 10^{-6} \rho^2 + 1.00 \cdot 10^{-04} \rho + 4.00 \cdot 10^{-01} \quad (6.6)$$

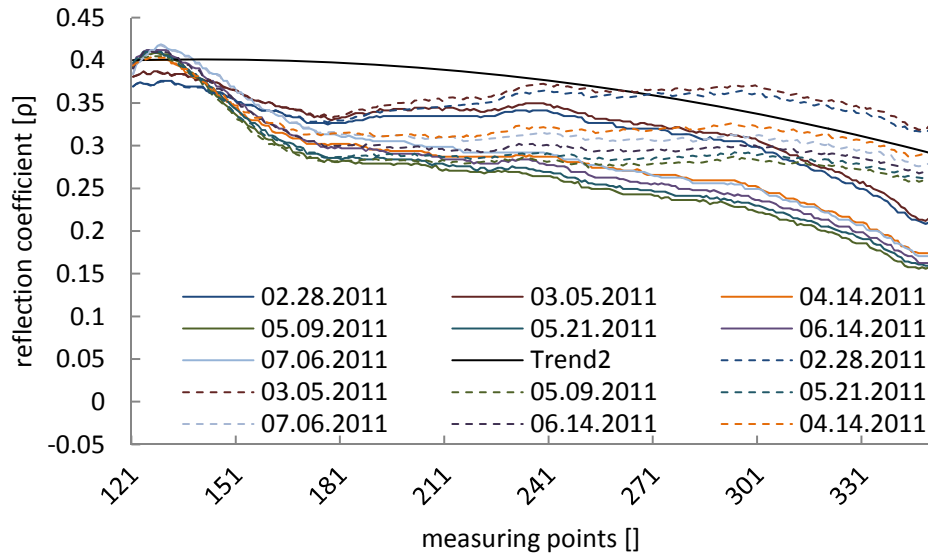


**Fig. 6.26.:** Signals from several measurements: Originals lined, Detrended dashed.

A comparison of them before and after detrending is given in fig. 6.26. Some measuring dates were picked from the entirety of data. It is not important to identify each of the signals. They shall rather show tendencies of the detrending results.

The upper sand layers are less detrended than the deeper ones. Due to a lack of reference data by missing liner samples this function could not be verified. Further laboratory experiments are necessary to verify this work step (chapter 8).

The resulted values ( $\rho_{detrended}$ ) were placed to the Tube calibration equation 6.5.

Chapter 6.4 describes furthermore a distinctive jitter between March and May that cannot be completely explained. However it can be assumed that this influence is not part of the hydraulic flow. Accordingly it was eliminated by whole day averages.

The spatial resolved VWC for all measurements from March till July is displayed in fig. 6.27. The ordinate shows the depth beneath ground level. The different colors are related to the soil moisture. The time related air temperature and precipitation supports the interpretation.

The patterns from fig. 6.23 and 6.25 can be clearly reconstructed. The ground surface near level tends to become drier in the course of spring. That correlates with

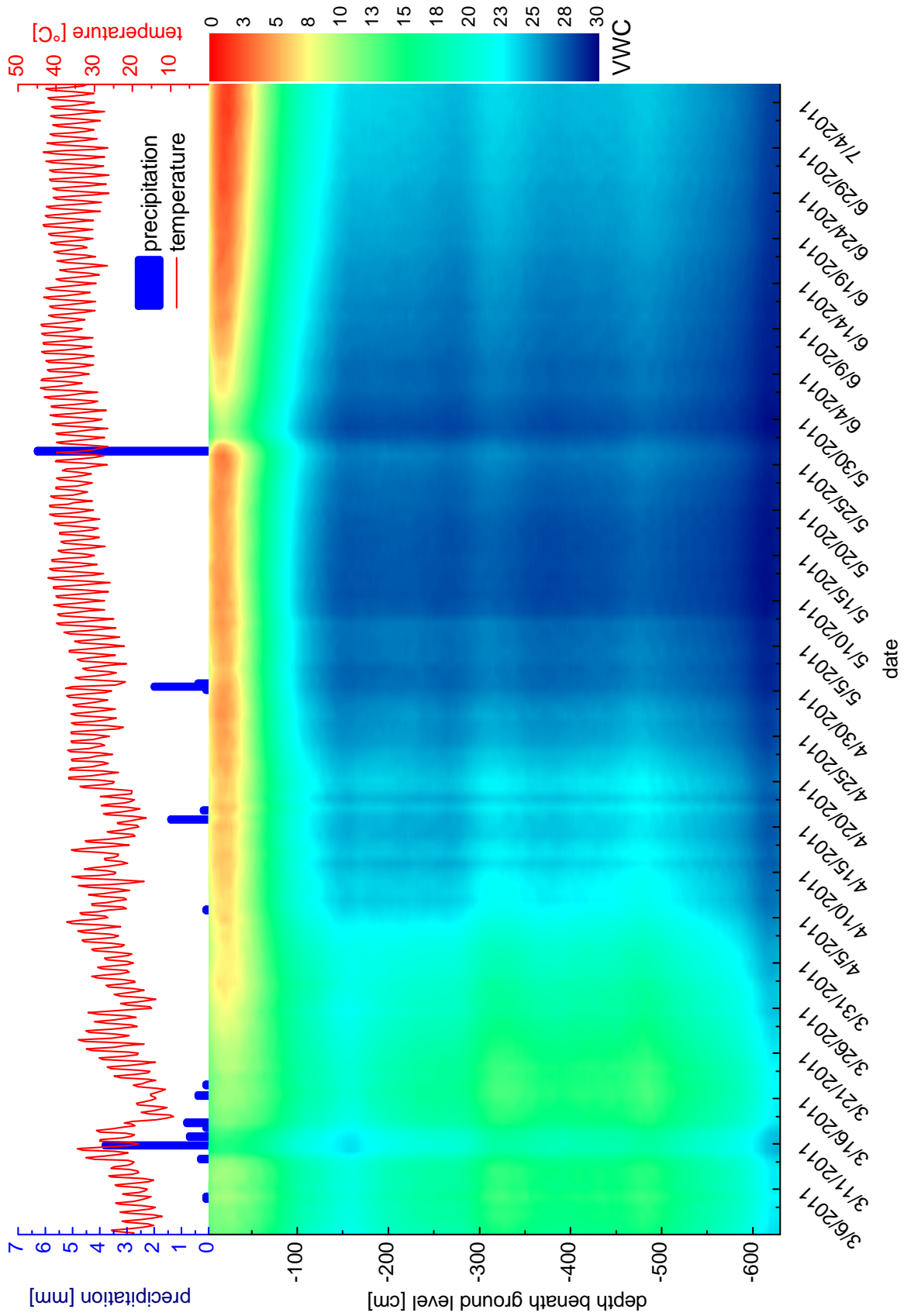


**Fig. 6.27.:** Spatial resolved sand moisture content from the beginning of March till the beginning of July; Air temperature and precipitation for the same period.

the increasing air temperature which is given above. The only disruptions occur during the precipitation events.

The two April rainfalls do not significantly change the soil moisture situation. Just the ground surface is slightly influenced. Consequently a minimum water amount between three and six millimeter precipitation seems to be necessary to moisturize the ground to deeper layers.

In contrast the March and May events change the soil moisture much more. They can be even detected in greater depths. Indeed it is suspicious that the change of soil moisture occurs simultaneous in all depths. Presumably preferential flow along the Tube sensor is responsible for this characteristic.

Like mentioned in section 6.4 the period between March and May is characterized by a significant sub surficial increase of soil moisture which cannot be explained with precipitation.

Accordingly the soil moisture increases slightly from the beginning of the monitoring till the May 11th, 2011 where the maximum soil moisture occurs. From then on moisture content decreases again till the end of the observation. This drying is just disrupted by the remoisturization during the May rainfall.

The reason for this asymmetric development until the reverse date seems to be a lateral, sub surficial outflow of the center pivot. By interpreting this assumption the irrigation lasted until the period of May 11th, 2011. Maybe a little bit earlier, because the soil is sluggishness of the soil. Probably the harvest took place with the ending irrigation. further interpretation of the other sensors will expose the influence of the center pivot.

Summarizing this assumption the moisture contents do not show erroneous values which could be supposed by considering the precipitation *only*. Indeed, it seems that the irrigation of the center pivot has a large lateral influence to its surrounding sediment bulk and therefore the soil moisture content of the test field.

Another considerable feature of fig. 6.27 can be seen in depth level 3.30 m and round 5 m. This zone is characterized by generally less soil moisture contents. The reason should be rather attributed to hydraulic properties of the sand. Presumably the grain sizes are bigger, therefore the water infiltrates faster through this layer. An error due to exaggerated detrending could be excluded, the anomaly is also given in the original data.

This assumption also explains the moisture content disruption during the March precipitation. The water passes this section faster, therefore the moisture content is less developed.

Whether the *calculated* data are right or wrong and how close they are to the real conditions can hardly be verified with the available data. Both the missing soil samples as well as the assumed hydraulic influence of the center pivot are responsible. However the *changes* of the spatial moisture distribution can be described sufficiently.

## 7. Conclusion of the Thesis

This diploma thesis has shown a complete way of measuring with TDR from theory, across field work, the calibration of sensors and the analysis of the results.

Chapter 5.2 describes the installation of the Taupe and Tube sensor systems. The test field was chosen on a farm near Riyadh. The location was characterized by several meters large sand sediments. Few meters next to the test field a center pivot was located.

Especially the Tube sensor left less doubt on the advantages of its construction. The installation as well as the sensor system is technically matured. Indeed, the placing to ground needs sophisticated direct push machines, which requires complex logistics. In contrast, the conceptual installation of the Taupe system seems a little bit more flexible.

The standard TDR measuring relates to the travel time of an electromagnetic impulse to soil moisture content. Due to the design of the sensors standard calibration functions could not be used to reach reliable output (*integral* VWC). The calibration of the sensors was passed in a couple of laboratory experiments (chapter 5.3.4, 6.2.2). The standardized thermogravimetric method was used as a reference. Theoretically predicted values supported these results. The spatial resolution was monitored with a self made short rod TDR-sensor (chapter 5.3.3, 6.2.1). A further challenge was the determination of the offset—the physical part between cable and sensor. It appeared in the signal as a high rise step. Even little changes generated systematic errors while extrapolating the travel time in air from the one meter long laboratory sensors to the much longer field sensors.

The spatial distribution of water was determined by the indirect dependency of the reflection coefficient ( $\rho$ ) from water content. Due to the EC of tap water an attenuation to the signal was found, which increased with moisture content (chapter 6.2.3). Based on the nature of the two sensor types this influence to Taupe was less than to the Tube system. This difference was referred to the fully coated wires of Taupe. Similarly this sensor is less sensitive to soil moisture changes. The influence was eliminated by detrending. These calculated values could be used to derive another calibration function. This was rechecked by calculating all reflection coefficients of the several signals to

---

*spatial* VWC's. Afterwards the measures of the short rod sensor were compared with these values. As a result it can be assumed that higher VWC's (15 vol % – 17 vol %) can be calculated more precise than lower moisture contents (0 vol % – 10 vol %).

The field measured signals were figured out to calculate the *integral* as well as the *spatial* VWC. In a long term view the six vertical sensors integral VWC showed differences among each other (chapter 6.3). Various parameters could therefore be the reason. However, the integral VWC within the same sensors differ just in a range of 2% or 3%. In the longterm observation from March – July 2011 the results next to the center pivot tended to increase slightly. It is assumed that the irrigation of the center pivot is the reason.

The spatial resolution of water content was calculated for only one of the vertical sensors (chapter 6.4, 6.5). The signals were analyzed before and after the detrending process to control the calculation. The soil moisture showed an anomaly from March till May 2011. Without measured precipitation the soil moisture decreased at the ground level, which corresponded to higher temperatures and a longer lasting drought. Indeed the soil moisture deeper than one meter increased steadily. From the end of May till the end of the monitoring the moisture content again developed synchronous. Likewise from these observations an influence of the center pivot on the test field could be concluded.

The irrigation also took place in February during the second field trip. It can therefore be assumed that the conditions at the beginning of the monitoring are not natural as well.

It can be stated that due to these hydraulic influences the main questions of the thesis could not be answered sufficiently because the sand does not consist of a representative soil moisture. A complete chain from precipitation to infiltration to drying through could not be observed.

However, the infiltration after the four precipitation events show that rain amounts of less than three till six millimeter rain are not able to infiltrate to deeper layers. Therefore the question about the propagated point of no return even remains unanswered. Indeed, the assumed coarse grained layer could serve as a capillary barrage.

## 8. Final Consideration and Future Prospects

A possibility to work further in this topic could be the improvement of the calibration of (chapter 6.2.2). An extension to 30–40 moisturization cycles could give a better reliability.

Furthermore a calibration series should be initiated with *different* moist sand within the single moisturization cycles. The profit would be an enhanced knowledge about the signal attenuation and how to handle that. Variations with different material properties are likely to follow.

For the thesis just one of the six sensors was analyzed. The next challenge should be to generate results for the rest of them. It can be expected that the moisture profile emerges rooftop-like downwards from the center pivot.

The next year will show, whether the center pivot will be cultivated and the artificial irrigation happens. If not, that could be a chance to observe complete rain – infiltration processes *without* external hydraulic effects.

Furthermore there is the possibility to moisturize the test field with the integrated irrigation construction during the drought. By repairing the damaged Taupe sensor it should be possible to involve this different sensor type to the analyzes to reach a higher reliability.

Another proposal for further improvement steps with large scale sensors would be a construction of a variance of the field used sensor. Both sensor types—Taupe and Tube—consist of advantages compared to each other. A combination of them could lead to an improvement of this technique.

## Bibliography

- M. F. Al-Rashed and M. M. Sherif. Water resources in the gcc countries: An overview. *Water Resources Management*, (14):59–75, 2000.
- D. Bänninger, H. Wunderli, M. Nussberger, and H. Flühler. Inversion of tdr signals—revisited. *Journal of Plant Nutrition and Soil Science*, 171(2):137–145, 2008. ISSN 14368730.
- H. K. Barth and K. Schliephake, editors. *Saudi-Arabien*. Perthes, 1997, Gotha und Stuttgart, 1998. ISBN 3623006890.
- Britannica Online Encyclopedia. Saudi arabia, 2011. URL <http://www.britannica.com/EBchecked/topic/525348/Saudi-Arabia>. 15.08.2011.
- Central Intelligence Agency. The world factbook, 2011. URL <https://www.cia.gov/library/publications/the-world-factbook/geos/sa.html>. 28.07.2011.
- O. Dahan. Flexible probe for measuring moisture content in soil, 2003. US 2003/0071637 A1.
- J. L. Davis and W. J. Chudobiak. In-situ meter for measuring relative permittivity of soils. *Geological Survey of Canada*, (75-1A):75–79, 1975.
- T. Dincer, A. Al-Mugrin, and U. Zimmermann. Study of the infiltration and recharge through the sand dunes in arid zones with special reference to the stable isotopes and thermonuclear tritium. *Journal of Hydrology*, (23):79–109, 1974.
- C. Dirksen. *Soil physics measurements*. Catena, Reiskirchen, Germany, 1999. ISBN 3-923381-43-3.
- S. R. Evett, J. A. Tolk, and T. A. Howell. Time domain reflectometry laboratory calibration in travel time, bulk electrical conductivity, and effective frequency. *Vadose Zone Journal*, (4):1020–1029, 2005.

- U. Kaatz and C. Hübner. Electromagnetic techniques for moisture content determination of materials. *Measurement Science and Technology*, 21(8):26p, 2010. ISSN 0957-0233.
- Ministry of Agriculture and Water. Climate atlas of saudi arabia, 1988.
- K. M. O'Connor and C. M. Dowding. *Geomeasurements by pulsing TDR cables and probes*. CRC Press, Boca Raton, 1999. ISBN 0-8493-0586-1.
- pk tools. Taupe data analysis, 2006.
- H. Römer. *Niederschlagsbestimmung aus Fernerkundungsdaten*. GRIN Verlag GmbH, München, 2007. ISBN 3638670287.
- K. Roth, R. Schulin, H. Flüßler, and W. Attinger. Calibration of time domain reflectometry for water content measurement using a composite dielectric approach. *Water Resources Research*, 26(10):2267, 1990. ISSN 0043-1397.
- D. L. Rowell. *Bodenkunde: Untersuchungsmethoden und ihre Anwendungen*. Springer, Berlin, 1997. ISBN 3540618252.
- A. Scheuermann, J. Brauns, S. Schlaeger, R. Becker, and C. Hübner. Monitoring von dämmen und deichen mittels tdr. In K. Kupfer and E. Trinks, editors, *Feuchtemessung - ein vielfältiges Problem mit großen Perspektiven*, pages 187–197, Weimar, 2002.
- C. Schüth, A. Kallioras, M. Piepenbrink, H. Pflöschinger, H. Al-Ajimi, I. Engelhardt, R. Rausch, and M. Al-Saud. New approaches to quantify groundwater recharge in arid areas. In *4th International Conference on Water Resources and Arid Environments (ICWRAE 4)*, volume 4, pages 325–329, 2010.
- M. Shahin. *Water resources and hydrometeorology of the Arab region*. Springer, Dordrecht, 2007. ISBN 1-4020-4577-8.
- M. Stacheder. *Die Time Domain Reflectometry in der Geotechnik: Messung von Wassergehalt, elektrischer Leitfähigkeit und Stofftransport*. PhD thesis, Universität Karlsruhe, Karlsruhe, 1996.
- M. Stacheder, F. Koeniger, and R. Schuhmann. New dielectric sensors and sensing techniques for soil and snow moisture measurements. *Sensors*, 9(4):2951–2967, 2009. ISSN 1424-8220.

- A. M. Subyani. Methods of groundwater recharge estimation in arid regions, 2005.
- G. C. Topp, J. L. Davis, and A. P. Annan. Electromagnetic determination of soil water content: measurements in coaxial transmission lines. *Water Resources Research*, (16):574–582, 1980.
- UN. Un millenium report: Chapter 4, 2002. URL <http://www.un.org/millennium/sg/report/ch4.pdf>. 07.03.2011.
- UN. The millenium development goals report 2010, 2010. URL <http://www.un.org/millenniumgoals/pdf/MDG%20Report%202010%20En%20r15%20-low%20res%2020100615%20-.pdf>. 07.03.2011.
- P. J. Vincent. *Saudi Arabia: An environmental overview*. Taylor & Francis, London, New York, 2008. ISBN 9780415413879.

## A. Appendix

**Listing A1.1:** Source code for 11 TAUPE-TDR-Sensors and 7 temperature sensors CS T107 in crbasic for Campbell Scientific Datalogger CR1000, edited by Franz Königer at August, 10th 2009, modified by Andreas Meier, at October, 18th 2010.

```
Public Batt_Volt
Public PTemp_C
Public WavePT(810)
Public MuxChan
Public T107_C_1
Public T107_C_2
Public T107_C_3
Public T107_C_4
Public T107_C_5
Public T107_C_6

Units Batt_Volt=Volts
Units PTemp_C=Deg C
Units T107_C_1=Deg C
Units T107_C_2=Deg C
Units T107_C_3=Deg C
Units T107_C_4=Deg C
Units T107_C_5=Deg C
Units T107_C_6=Deg C

DataTable(T_Batt, True, -1)
    DataInterval(0,4,Hr,10)
    Sample(1,Batt_Volt,FP2)
    Sample(1,PTemp_C,FP2)
EndTable
```

---

```

DataTable (TabTemp , True , -1)
    DataInterval (0,4,Hr ,10)
    Sample (1, T107_C_1 , FP2)
    Sample (1, T107_C_2 , FP2)
    Sample (1, T107_C_3 , FP2)
    Sample (1, T107_C_4 , FP2)
    Sample (1, T107_C_5 , FP2)
    Sample (1, T107_C_6 , FP2)
EndTable

DataTable (TDR_Wave , 1 , -1)
    Sample (1, MuxChan , FP2)
    Sample (810, WavePT () , FP2)
EndTable

BeginProg
    SDMSpeed (50)

    Scan (4, Hr , 1, 0)
        Battery (Batt_Volt)
        PanelTemp (PTemp_C , _50Hz)
        CallTable (T_Batt)

        Therm107 (T107_C_1 , 1, 1, 1, 0 , _60Hz , 1, 0)
        Therm107 (T107_C_2 , 1, 2, 1, 0 , _60Hz , 1, 0)
        Therm107 (T107_C_3 , 1, 3, 1, 0 , _60Hz , 1, 0)
        Therm107 (T107_C_4 , 1, 4, 1, 0 , _60Hz , 1, 0)
        Therm107 (T107_C_5 , 1, 5, 2, 0 , _60Hz , 1, 0)
        Therm107 (T107_C_6 , 1, 6, 2, 0 , _60Hz , 1, 0)
        CallTable (TabTemp)

    SW12 (1)
    Delay (0, 2, Sec)

```

---

```
        MuxChan=2001
TDR100(WavePT(),0,1,2001,32,0.67,801,19.0,30.0,2.0,0.035,1,0)
CallTable TDR_Wave()
        MuxChan=3001
TDR100(WavePT(),0,1,3001,32,0.67,801,29.0,30.0,0,0.035,1,0)
CallTable TDR_Wave()
        MuxChan=4001
TDR100(WavePT(),0,1,4001,32,0.67,801,3.5,4.0,2.0,0.035,1,0)
CallTable TDR_Wave()
        MuxChan=5001
TDR100(WavePT(),0,1,5001,32,0.63,801,7.5,25.0,2.0,0.035,1,0)
CallTable TDR_Wave()
        MuxChan=6001
TDR100(WavePT(),0,1,6001,32,0.63,801,16.0,17.0,2.0,0.035,1,0)
CallTable TDR_Wave()
        MuxChan=8001
TDR100(WavePT(),0,1,8001,32,0.63,801,8.5,18.0,2.0,0.035,1,0)
CallTable TDR_Wave()
        MuxChan=1101
TDR100(WavePT(),0,1,1101,32,0.63,801,13.0,14.0,2.0,0.035,1,0)
CallTable TDR_Wave()
        MuxChan=1201
TDR100(WavePT(),0,1,1201,32,0.63,801,13.0,20.0,2.0,0.035,1,0)
CallTable TDR_Wave()
        MuxChan=1301
TDR100(WavePT(),0,1,1301,32,0.63,801,15.0,15.0,2.0,0.035,1,0)
CallTable TDR_Wave()
        MuxChan=1401
TDR100(WavePT(),0,1,1401,32,0.63,801,16.0,18.0,2.0,0.035,1,0)
CallTable TDR_Wave()
```

```
        SW12(0)
        NextScan
EndProg
```

---

**Tab. A.1.:** Added tap water in the single moisturization cycles (chapter 5.3.4).

No.	water amount [l]	water amount [mm]
1	0.0	0.0
2	1.0	2.8
3	1.3	3.6
4	1.6	4.4
5	1.9	5.3
6	2.2	6.1
7	2.5	6.9
8	2.8	7.8
9	3.1	8.6
10	3.4	9.4
11	3.7	10.3
12	4.0	11.1
13	4.3	11.9
14	4.6	12.8
15	4.9	13.6
16	5.2	14.4
17	5.5	15.3
18	5.8	16.1
19	6.1	16.9
20	6.4	17.8

**Tab. A.2.:** VWC of Z 5: Thermogravimetric results, calculation with Topp's equation and a 3rd order polynomial as well as theoretical VWC calculated from controlled water add-on, according graph in fig. 6.4, pg. 29.

No.	thermograv. determined $\Theta_{vol}\%$	Topp's equation $\Theta_{vol}\%$	Cal.fct. <sup>3</sup> $\Theta_{vol}\%$	moisturization amount $\Theta_{vol}\%$
1	0.0	1.6	0.2	0.0
2	4.7	5.7	6.5	3.5
3	5.6	4.8	5.2	4.6
4	6.8	5.1	5.6	5.6
5	7.9	6.9	8.0	6.7
6	9.1	7.4	8.6	7.7
7	10.2	9.0	10.4	8.8
8	11.3	9.9	11.3	9.8
9	12.3	10.0	11.4	10.9
10	12.8	11.9	13.1	11.9
11	14.0	13.1	14.1	13.0
12	13.6	13.1	14.2	14.0
13	15.6	14.6	15.2	15.1
14	16.7	16.9	16.8	16.1
15	17.3	18.4	17.7	17.2
16	19.1	19.9	18.6	18.3
17	19.8	22.9	20.5	19.3
18	21.0	22.7	20.3	20.4
19	21.8	24.9	22.1	21.4
20	22.6	25.3	22.5	22.5

**Tab. A.3.:** Calculated volumetric water content from chapter 6.2.1, measured with sensor Z 5, the values are displayed in fig. 6.4 and 6.5.

No.	P1	P2	P3	P4	P5	<i>average P1-P5</i>	standart deviation
	$\Theta_{vol}\%$	$\Theta_{vol}\%$	$\Theta_{vol}\%$	$\Theta_{vol}\%$	$\Theta_{vol}\%$	$\Theta_{vol}\%$	$\Theta_{vol}\%$
1	-4.2	2.3	0.6	1.3	0.6	0.1	2.3
2	5.3	7.5	6.0	7.7	5.7	6.5	1.0
3	7.0	1.0	5.9	6.1	5.7	5.1	2.1
4	3.0	7.7	2.4	7.1	7.2	5.5	2.3
5	8.2	8.8	7.8	7.2	8.1	8.0	0.5
6	8.0	9.3	8.6	9.0	8.1	8.6	0.5
7	9.5	10.8	10.6	10.1	10.9	10.4	0.5
8	11.9	10.9	11.4	11.9	10.5	11.3	0.6
9	11.8	10.3	12.0	12.0	10.6	11.3	0.7
10	13.9	13.7	13.2	12.3	12.4	13.1	0.6
11	14.8	13.7	13.7	14.5	13.7	14.1	0.5
12	15.2	13.7	14.6	14.3	12.7	14.1	0.9
13	16.3	15.3	15.3	14.4	14.8	15.2	0.6
14	17.3	16.1	16.0	16.7	17.6	16.8	0.7
15	17.3	17.4	18.8	17.2	17.7	17.7	0.6
16	19.9	17.4	18.5	18.5	18.5	18.6	0.8
17	20.8	19.6	21.8	20.2	20.0	20.5	0.8
18	21.0	21.1	19.1	20.0	20.6	20.4	0.7
19	21.1	22.2	22.1	22.6	22.5	22.1	0.5
20	23.8	23.7	22.4	21.0	21.8	22.5	1.1

**Tab. A.4.:** Travel time and  $K_a$  of Taupe sensor measures in sandbox experiment II, travel time in air and offset in tab. 2.1, pg. 29, VWC ( $\Theta_{vol}\%$ ) calculated with equation 6.2.

No.	$t_m$ [ns]	$t_m$ offset corrected [ns]	$\sqrt{K_a}$	$K_a$	$\Theta_{vol}\%$
1	4.731	4.338	1.161	1.347	2.1
2	4.761	4.367	1.169	1.366	2.7
3	4.889	4.495	1.203	1.447	5.0
4	4.986	4.593	1.229	1.510	6.7
5	5.064	4.670	1.250	1.562	8.0
6	5.140	4.747	1.270	1.613	9.3
7	5.197	4.803	1.285	1.652	10.3
8	5.365	4.972	1.330	1.770	12.9
9	5.280	4.886	1.308	1.710	11.6
10	5.407	5.014	1.342	1.800	13.6
11	5.490	5.096	1.364	1.860	14.7
12	5.422	5.029	1.346	1.811	13.8
13	5.464	5.071	1.357	1.841	14.4
14	5.603	5.209	1.394	1.943	16.3
15	5.697	5.304	1.419	2.014	17.5
16	5.700	5.306	1.420	2.016	17.6
17	6.017	5.623	1.505	2.264	21.0
18	6.097	5.704	1.526	2.329	21.7
19	6.049	5.655	1.513	2.290	21.3
20	6.127	5.733	1.534	2.353	21.9

**Tab. A.5.:** Travel time and  $K_a$  of Tube sensor measures in sandbox experiment II, travel time in air and offset in tab. 2.1 pg. 29, VWC ( $\Theta_{vol}\%$ ) calculated with equation 6.2.

No.	$t_m$ [ns]	$t_m$ offset corrected [ns]	$\sqrt{K_a}$	$K_a$	$\Theta_{vol}\%$
1	5.127	4.813	1.195	1.427	1.2
2	5.324	5.009	1.243	1.546	3.1
3	5.567	5.253	1.304	1.700	5.4
4	5.726	5.411	1.343	1.804	6.9
5	5.787	5.473	1.359	1.846	7.5
6	6.020	5.705	1.416	2.006	9.7
7	6.057	5.743	1.426	2.032	10.1
8	6.289	5.974	1.483	2.199	12.2
9	6.269	5.955	1.478	2.185	12.0
10	6.388	6.074	1.508	2.273	13.0
11	6.608	6.293	1.562	2.440	14.9
12	6.557	6.242	1.550	2.401	14.5
13	6.603	6.288	1.561	2.437	14.9
14	6.765	6.451	1.601	2.564	16.2
15	6.756	6.441	1.599	2.557	16.1
16	7.098	6.783	1.684	2.835	18.8
17	7.306	6.992	1.736	3.012	20.3
18	7.028	6.714	1.667	2.777	
19	7.729	7.415	1.841	3.387	
20	8.082	7.768	1.928	3.718	

**Tab. A.6.:** Physical length of the Tube sensors compared to its travel times in air ( $t_l$ ).

name	length [cm]	$t_l$ [ns]
V1	774	31.498
V2	515	21.063
V3	630	25.697
V4	640	26.100
V5	565	23.078
V6	515	21.063

## Acknowledgements

This diploma thesis was generated on the Helmholtz–Centre of Environmental Research UFZ in the department Catchment Hydrology. Within the IWAS project it was possible for me to write my thesis in a non university scientific context.

I would like to thank Prof. Dr. Arno Kleber<sup>1</sup> for providing support and helpful advice and the permission to write this thesis on the UFZ.

Special thanks goes to Dr. Tino Rödiger<sup>2</sup> for his great supervising, inspiring discussions, critics and not least the review of this work.

Not less I would like to thank Dipl.-Ing. Franz Königer<sup>3</sup>, who introduced me to TDR measuring technique. Without his broad and patient explanations to technical and physical questions this thesis would hardly have been possible.

I would also like to express my thanks to Prof. Dr. Randolf Rausch<sup>4</sup> who provided the possibility of field work in Saudi Arabia within an internship at the GTZ.

Furthermore my thanks goes to Dr. Christian Siebert<sup>2</sup>, Oliver Thiel<sup>2</sup> and Dr. Andreas Kallioras<sup>6</sup> for the professional and successful cooperation during the field work and the construction of the test field.

Tobias Fuest<sup>5</sup> has been collecting data from the field data loggers since March 2011. I wish to thank him as well.

For the linguistic revision of the thesis my sincere thanks goes to Evelyn Braun.

My parents provided me moral and financial support throughout my whole education. They offered me the chance to take opportunities when I had them. THANK YOU!

Last but not least I would like to thank my son Lorenz for his ability to distract me in a non-academic way and of course my girlfriend Christiane for her encouragement and her love.

---

<sup>1</sup>Technische Universität Dresden – Institute of Geography

<sup>2</sup>Helmholtz–Centre of Environmental Research UFZ

<sup>3</sup>Karlsruhe Institute of Technology – Institute of Functional Interfaces

<sup>4</sup>TU Darmstadt – Institute of Applied Geosciences

<sup>5</sup>GTZ–IS

<sup>6</sup>National Technical University of Athens, School of Mining and Metallurgical Engineering, Section of Geological Sciences

## Statement of Authorship/ Selbstständigkeitserklärung

Hiermit erkläre ich, dass ich die Diplomarbeit selbstständig verfasst habe und keine anderen als die angegebenen Quellen und Hilfsmittel benutzt habe. Alle Stellen der Arbeit, die wörtlich oder sinngemäß aus Veröffentlichungen oder aus anderweitigen fremden Äußerungen entnommen wurden, sind als solche gekennzeichnet. Ferner erkläre ich, dass die Arbeit noch nicht in einem anderen Studiengang als Prüfungsleistung verwendet wurde.

I hereby certify that this diploma thesis has been composed by myself. I did not use other literature and devices as denoted. All references and verbatim extracts have been quoted, and all sources of information have been specifically acknowledged. The thesis has not been accepted in any previous application for a degree.

Ort, Datum/ Place, Date

Unterschrift/ signature

Dresden, October 20, 2011

\_\_\_\_\_

Ich bin damit einverstanden, daß die Arbeit nach positiver Begutachtung der Sächsischen Landesbibliothek Staats- und Universitätsbibliothek Dresden zur Verfügung gestellt wird.

After positive appraisal of this thesis, I agree that one copy of my presented thesis may remain at the disposal of the Saxon State and University Library Dresden.

Ort, Datum/ Place, Date

Unterschrift/ signature

Dresden, October 20, 2011

\_\_\_\_\_